Available online at www.sciencedirect.com
ScienceDirect
Journal of Computational Physics 227 (2008) 7561–7586
JOURNAL OF COMPUTATIONAL PHYSICS
www.elsevier.com/locate/jcp

Semi-implicit time integration for P_N thermal radiative transfer

Ryan G. McClarren [a,*], Thomas M. Evans [b], Robert B. Lowrie [a], Jeffery D. Densmore [a]

[a] Computational Physics Group (CCS-2), Los Alamos National Laboratory, P.O. Box 1663, MS D413, Los Alamos, NM 87545[1], United States

[b] Reactor Analysis Group, Oak Ridge National Laboratory, P.O. Box 2008, MS 6172, Oak Ridge, TN 37831, United States

Received 8 August 2007; received in revised form 14 February 2008; accepted 22 April 2008
Available online 7 May 2008

Abstract

Implicit time integration involving the solution of large systems of equations is the current paradigm for time-dependent radiative transfer. In this paper we present a semi-implicit, linear discontinuous Galerkin method for the spherical harmonics (P_N) equations for thermal radiative transfer in planar geometry. Our method is novel in that the material coupling terms are treated implicitly (via linearizing the emission source) and the streaming operator is treated explicitly using a second-order accurate Runge–Kutta method. The benefit of this approach is that each time step only involves the solution of equations that are local to each cell. This benefit comes at the cost of having the time step limited by a CFL condition based on the speed of light. To guarantee positivity and avoid artificial oscillations, we use a slope-limiting technique. We present analysis and numerical results that show the method is robust in the diffusion limit when the photon mean-free path is not resolved by the spatial mesh. Also, in the diffusion limit the time step restriction relaxes to a less restrictive explicit diffusion CFL condition. We demonstrate with numerical results that away from the diffusion limit our method demonstrates second-order error convergence as the spatial mesh is refined with a fixed CFL number.

Keywords: Thermal radiative transfer; P_N approximation; Discontinuous Galerkin; Asymptotic diffusion limit

1. Introduction

Thermal radiative transfer by X-ray-regime radiation is an intrinsic component of coupled radiation–hydrodynamics problems. The independent variables of the transport equation governing thermal radiative transfer are position, angle, frequency, and time. This dependence on a seven-dimensional phase space leads to expensive memory and computer-time requirements. Additionally, because radiation travels at the speed of light and the corresponding CFL limit on time-step size for time-explicit schemes is very restrictive, state-of-the-art

[1] Los Alamos National Laboratory is operated by Los Alamos National Security, LLC for the U.S. Department of Energy under Contract DE-AC52-06NA25396.

* Corresponding author. Tel.: +1 505 665 1397.
E-mail address: ryanmc@lanl.gov (R.G. McClarren).

0021-9991/$ - see front matter © 2008 Elsevier Inc. All rights reserved.
doi:10.1016/j.jcp.2008.04.029

transport methods use implicit schemes, which require the solution of large systems of equations each time step. For these reasons, radiation–hydrodynamics calculations are often limited to low-order angular approximations, such as diffusion, for simulating thermal radiative transfer.

Transport methods that are higher order in angle can be classified as either deterministic or stochastic. Of deterministic methods, the current state-of-the-art is the discrete-ordinates (S_N) method utilizing Diffusion Synthetic Acceleration (DSA) as a preconditioner within a Krylov iterative framework [1]. The most widely used stochastic, or Monte Carlo, method is the Implicit Monte Carlo (IMC) scheme of Fleck and Cummings [2]. Deterministic methods based on the second-order form of the radiation-transport equation have also been developed [3].

Discrete-ordinates methods for thermal radiative transfer have several drawbacks. First and foremost, they suffer from ray-effects [4]. Also, inverting the transport operator involves performing a cell-based sweep in the direction of particle travel. Generalizing and parallelizing sweeps on anything but orthogonal, logically rectangular meshes is complicated and difficult to implement. Time-dependent calculations require the storage of angular information, a situation that results in $O(N^2)$ unknowns per cell in multidimensional simulations, where N is the order of the S_N approximation.

Finally, the solution procedure for S_N schemes is very complex. A typical solution requires an outer iteration (GMRES or Gauss-Seidel) over frequency, and within each outer iteration a set of nested inner iterations (GMRES or Richardson) that includes sweeps and solving a diffusion equation for DSA preconditioning. Given that the sweep itself is highly specialized to the mesh topology and parallel decomposition, implementation can be onerous and is generally not extensible.

Monte Carlo methods provide high angular fidelity; however, they are computationally expensive because accurate solutions require an adequate sampling of the problem phase space. This requirement is typically $O(10)$ particles per cell per frequency group. Also, simulations of coupled radiation hydrodynamics that employ Monte Carlo are difficult to parallelize efficiently because hydrodynamics calculations prefer spatial decomposition, whereas pure particle Monte Carlo works best with particle decomposition and spatial replication. Spatially decomposed Monte Carlo methods can suffer from severe load imbalance.

Another technique that has been used to deterministically solve the radiation-transport equation is the P_N method. This method involves expanding the angular dependence of the radiation intensity, the fundamental unknown of the transport equation, in spherical harmonics. The result is a system of coupled equations for the angular moments of the radiation intensity. This technique has, until recently, not been considered viable for multidimensional problems because the transport operator cannot be inverted efficiently [5]. Recent work [6–10] has shown how implicit time integration with Riemann solvers can be efficiently used for the P_N equations. However, implicit methods for P_N are, at present, not as efficient as implicit S_N methods. Also, in multidimensional problems the P_N equations have nullspace issues with zero eigenvalues that are not advected by an upwind scheme [11].

The spatial discretization we will be concerned with in this paper is the discontinuous Galerkin method. This method was first developed by Reed and Hill for solving the neutron transport equation [12]. Cockburn and Shu showed that using explicit, Runge–Kutta time integration with discontinuous Galerkin spatial discretization gives a total variation bounded method when a slope limiter is used [13]. Along those lines, Lowrie and Morel applied the Runge–Kutta discontinuous Galerkin method to radiation hydrodynamics under the P_1 approximation [14]. Parallel to this work implicit P_N methods using a finite volume method were investigated [6–9,15].

Below we develop a semi-implicit method for the P_N equations where we time-integrate the streaming terms explicitly with a second-order accurate Runge–Kutta method and the material-coupling terms implicitly; this methodology is a generalization of the P_1 discretization in Ref. [14]. We implicitly treat the material-coupling terms because the material temperature can evolve on a time scale faster than the streaming time scale. The implicit system is local to each element, and with a linearization of the material coupling terms this implicit integration is trivial.

A semi-implicit approach was also investigated by Klar [16] and Klar and Unterreiter [17]. Klar pointed out that a naive semi-implicit approach based on treating the streaming with forward Euler and the material-coupling terms with backward Euler would lead to an unsatisfactory scheme in the diffusion limit [16]. Refs. [16,17] then presented a splitting scheme that limited to a valid discretization of the asymptotic diffusion equa-

tion. This splitting scheme expands the intensity into an $O(1)$ even angular component and an $O(\epsilon)$ odd angular component, and uses a finite difference spatial discretization. To integrate time, certain material interaction terms are integrated implicitly, while all other terms are integrated explicitly. In the diffusion limit, this splitting scheme limits to a finite difference approximation with forward Euler time integration.

Our semi-implicit scheme differs from that presented by Klar in several ways. First, we treat all the material-coupling terms implicitly, where Klar's method treats the angularly integrated terms explicitly. Our finite element formulation is second-order accurate in space and time in the streaming limit, whereas Klar's is first order in space and time in the streaming limit. Finally, the discontinuous Galerkin method is widely used in the radiation transport community because of its robustness in the diffusion limit, therefore our semi-implicit scheme based on discontinuous finite elements can easily be integrated into existing radiation transport codes.

We were motivated to investigate a semi-implicit method to address the shortcomings of other transport methods in large-scale radiation–hydrodynamics simulations. While the semi-implicit approach has a CFL limit for the time-step size based on the speed of light this drawback is mitigated by the fact that, in realistic radiation–hydrodynamics problems, the time-step size is often limited to $O(10^{-11}\ \text{s})$ by the dependence of material properties on the material temperature. In large-scale problems run on massively parallel architectures, the efficiencies allowed by a semi-implicit approach (for example, very low communication requirements and ease of spatial decomposition) should make the cost of this new method competitive with existing transport methods. Beyond standard radiation hydrodynamics, we are also interested in fully relativistic radiation hydrodynamics where the hydrodynamic time scale is on the order of the speed of light. In these problems the radiation and hydrodynamic time scales are nearly equal, and there is no additional cost to treat radiation streaming explicitly.

This paper does not present computational cost comparisons between our method and other transport packages because in one dimension the efficiencies of this approach would not be realized. Rather, the goal of this paper is to demonstrate that such a method can give stable and accurate results for thermal radiative transfer.

We will show that the discontinuous Galerkin method with semi-implicit time integration does preserve the asymptotic diffusion limit of the thermal radiative transfer system – a characteristic that upwind finite volume P_N methods fail to achieve [15]. In this limit, our hyperbolic CFL time-step size restriction is relaxed to the stability limit of an explicit diffusion discretization similar to that of Klar's splitting scheme. Also, our time discretization in the diffusion limit is a one-step scheme rather than the doubly-lagged discretization that caused Klar to reject the naive semi-implicit discretization of the transport equation [16]. In essence, our method shows that this naive scheme could be corrected by using second-order accurate Runge–Kutta for the streaming terms.

We begin this paper with a derivation of the P_N equations for thermal radiative transfer. We then develop our discretization and present the asymptotic diffusion limit of the method. In Section 9 we present tests of the method on various problems to demonstrate its efficacy and confirm our asymptotic analysis. Finally in Section 10 we summarize our results and point out the way forward for extensions of this method.

2. Radiative-transfer equations

We begin with the equations that describe planar geometry thermal radiative transfer in the absence of scattering, external sources, and hydrodynamic motion [18]:

$$\frac{1}{c}\frac{\partial \psi}{\partial t} + \mu\frac{\partial \psi}{\partial x} + \sigma\psi = \sigma B, \tag{1}$$

$$\frac{\partial e}{\partial t} = 2\pi\sigma(\psi - B)\,\mathrm{d}\mu\,\mathrm{d}\nu. \tag{2}$$

Here, Eq. (1) is the radiation-transport equation, with $\psi(x,\mu,\nu,t)$ the specific intensity, x is the spatial variable, $\mu = \cos\theta$ with θ the angle between a photon's direction of flight and the x-axis, ν is the photon's frequency, and t is the time variable. The opacity is given by $\sigma(x,\nu)$. Eq. (2) is the material-energy equation

with e the material internal energy per volume. We define angular moments of the radiation intensity, $\psi \equiv \psi(x,\mu,v,t)$, as

$$E = \frac{2\pi}{c}\psi \,\mathrm{d}\mu\,\mathrm{d}v, \tag{3}$$

$$F = 2\pi\mu\psi \,\mathrm{d}\mu\,\mathrm{d}v, \tag{4}$$

$$P = \frac{2\pi}{c}\mu^2\psi \,\mu\,\mathrm{d}v. \tag{5}$$

In Eqs. (1) and (2), $B(v,T)$ is the Planck function such that

$$\int_v B \,\mathrm{d}v = \frac{acT^4}{4\pi}. \tag{6}$$

Here, T is the material temperature in keV, $c = 3\times10^8\,\mathrm{cm\,s^{-1}}$ is the speed of light, and $a = 1.372\times10^{14}\,\mathrm{ergs\,cm^{-3}\,keV^{-4}}$, is the radiation constant. The temperature is related to the internal energy through an equation of state, $e(\rho,T)$, where ρ is the material density. In this study we do not consider hydrodynamic motion, so ρ is constant, and we can rewrite the time derivative in Eq. (2) as

$$\frac{\partial e}{\partial t} = \frac{\partial e}{\partial T}\frac{\partial T}{\partial t} = C_v\frac{\partial T}{\partial t}, \tag{7}$$

where C_v is the heat capacity at constant volume. For convenience, we operate on Eq. (1) by $\int(\cdot)\,\mathrm{d}v$ and assume σ is independent of v to yield the frequency-independent grey transport equation,

$$\frac{1}{c}\frac{\partial\psi}{\partial t} + \mu\frac{\partial\psi}{\partial x} + \sigma\psi = \sigma\frac{acT^4}{4\pi} \tag{8}$$

and material energy equation,

$$\frac{\partial e}{\partial t} = c\sigma(E - aT^4). \tag{9}$$

Here, $\psi \equiv \psi(x,\mu,t)$. We will be working with the grey form of the radiation-transport equation in the remainder of this paper.

2.1. P_N equations

We will treat the angular dependence of Eq. (8) by expanding ψ in Legendre polynomials. This technique results in the so-called P_N equations, expressions that can be thought of as a series of orthonormal angular moments of Eq. (8). We expand ψ in Legendre polynomials according to

$$\psi(x,\mu,t) = \sum_{n=0}^{N}\frac{2n+1}{4\pi}P_N(\mu)\psi_n(x,t). \tag{10}$$

The moments are defined by

$$\psi_n(x,t) = 2\pi\int_{-1}^{1}P_N(\mu)\psi(x,\mu,t)\,\mathrm{d}\mu. \tag{11}$$

Now we can equate the moments of ψ to E, F, and P:

$$E = \frac{1}{c}\psi_0; \tag{12a}$$

$$F = \psi_1; \tag{12b}$$

$$P = \frac{1}{3c}\psi_0 + \frac{2}{3c}\psi_2. \tag{12c}$$

Substituting the Legendre polynomial expansion, Eq. (10), into the transport equation, Eq. (8), and using the orthogonality and recurrence relations for Legendre polynomials allows us to write the P_N equations as [19]

$$\frac{1}{c}\frac{\partial \psi_0}{\partial t}+\frac{\partial \psi_1}{\partial x}+\sigma\psi_0=\sigma acT^4, \tag{13a}$$

$$\frac{1}{c}\frac{\partial \psi_n}{\partial t}+\frac{\partial}{\partial x}\left(\frac{n}{2n+1}\psi_{n-1}+\frac{n+1}{2n+1}\psi_{n+1}\right)+\sigma\psi_n=0,\quad n>0. \tag{13b}$$

These equations represent an unclosed system due to the ψ_{n+1} term in Eq. (13b). The most common closure employed is to set this term to zero for $n=N$, i.e. $\psi_{N+1}=0$.

In terms of the P_N expansion, the material-energy equation is

$$\frac{\partial e}{\partial t}=\sigma(\psi_0-acT^4). \tag{14}$$

The material-energy equation added to the P_0 equation, Eq. (13a), gives an equation for the conservation of energy,

$$\frac{\partial}{\partial t}(E+e)+\frac{\partial F}{\partial x}=0, \tag{15}$$

that when integrated over a suitable spatial domain implies than any change in the total energy is due to boundary terms,

$$\frac{\partial}{\partial t}\int_{X^-}^{X^+}\mathrm{d}x\,(E+e)=F(X^-,t)-F(X^+,t), \tag{16}$$

where X^- and X^+ are the left and right edges of the system, respectively. These equations state that the only change in the net energy in the system is due to energy crossing the system boundaries.

3. Conservation form

The conservative form for Eq. (13) is

$$\frac{\partial \mathbf{u}}{\partial t}+\frac{\partial \mathbf{f}(\mathbf{u})}{\partial x}=\mathbf{q}(\mathbf{u}), \tag{17}$$

where $\mathbf{u}$ is the vector of unknowns, and $\mathbf{f}(\mathbf{u})$ is the flux vector. In our model $\mathbf{f}(\mathbf{u})$ is linear such that Eq. (17) can be written as

$$\frac{\partial \mathbf{u}}{\partial t}+\mathbf{A}\frac{\partial \mathbf{u}}{\partial x}=\mathbf{q}(\mathbf{u}). \tag{18}$$

We can cast Eq. (13) into this form by defining the following vectors and matrices,

$$\mathbf{u}=\begin{pmatrix}\psi_0\\ \psi_1\\ \psi_2\\ \vdots\\ \psi_N\end{pmatrix},\quad \mathbf{A}=\begin{pmatrix}0 & 1 & \dots & \dots & \dots & \dots & 0\\ \frac{1}{3} & 0 & \frac{2}{3} & \dots & \dots & \dots & 0\\ 0 & \frac{2}{5} & 0 & \frac{3}{5} & \dots & \dots & 0\\ \dots & \dots & \dots & \dots & \frac{N-1}{2N-1} & 0 & \frac{N}{2N-1}\\ \dots & \dots & \dots & \dots & \dots & \frac{N}{2N+1} & 0\end{pmatrix},\quad \mathbf{q}(\mathbf{u})=\begin{pmatrix}\sigma(acT^4-\psi_0)\\ -\sigma\psi_1\\ -\sigma\psi_2\\ \vdots\\ -\sigma\psi_N\end{pmatrix}, \tag{19}$$

and we have used the closure $\psi_{N+1}=0$. The elements of the matrix $\mathbf{A}$ can be defined more succinctly,

$$A_{i,j}=\begin{cases}\frac{n}{2n+1} & i=n,\ j=n-1,\ n\in[1,N],\\ \frac{n+1}{2n+1} & i=n,\ j=n+1,\ n\in[0,N-1],\\ 0 & i\neq n \text{ and } j\notin\{n-1,n+1\},\end{cases}$$
$$\forall\ i,j\in[0,N]. \tag{20}$$

Thus, each row $n\in[1,N-1]$ has two elements, and the $n=0$ and $n=N$ rows each have one element.

3.1. Eigensystem of **A**

In order to solve Eq. (18) the eigensystem of **A** will be required, a system of equations that is given by (see, for example, [20])

$$\mathbf{A} = \mathbf{R}\boldsymbol{\Lambda}\mathbf{R}^{-1}. \tag{21}$$

Here $\boldsymbol{\Lambda} = \mathrm{diag}(\lambda_0, \lambda_1, \ldots, \lambda_N)$ is the diagonal matrix of eigenvalues, and the matrix **R** is the column-wise matrix of eigenvectors, i.e.,

$$\mathbf{R} = (\mathbf{r}_0|\mathbf{r}_1|\ldots|\mathbf{r}_N). \tag{22}$$

As an example, the P_1 equations have the following definitions for **u**, **A**, and **q**,

$$\mathbf{u} = \begin{pmatrix} \psi_0 \\ \psi_1 \end{pmatrix}, \quad \mathbf{A} = \begin{pmatrix} 0 & 1 \\ \frac{1}{3} & 0 \end{pmatrix}, \quad \mathbf{q}(\mathbf{u}) = \begin{pmatrix} \sigma(acT^4 - \psi_0) \\ -\sigma\psi_1 \end{pmatrix}. \tag{23}$$

The eigenvalue/eigenvector matrices of **A** for this system are

$$\boldsymbol{\Lambda} = \begin{pmatrix} -\frac{1}{\sqrt{3}} & 0 \\ 0 & \frac{1}{\sqrt{3}} \end{pmatrix}, \quad \mathbf{R} = \begin{pmatrix} -\sqrt{3} & \sqrt{3} \\ 1 & 1 \end{pmatrix}, \quad \mathbf{R}^{-1} = \begin{pmatrix} -\frac{1}{2\sqrt{3}} & \frac{1}{2} \\ \frac{1}{2\sqrt{3}} & \frac{1}{2} \end{pmatrix}. \tag{24}$$

Higher-order P_N equations and corresponding eigensystems can be generated using the definition of the general **A** matrix in Eq. (20). The eigenvalues of a given P_N system are the zeros of the Legendre polynomial $P_{N+1}(\mu)$ [11]. With an eigenvalue denoted by λ_k, the eigenvectors are given by

$$\mathbf{r}_k = [P_0(\lambda_k), P_1(\lambda_k), \ldots, P_N(\lambda_k)]^{\mathrm{T}}. \tag{25}$$

For examples of the P_3 and P_5 systems of equations, see Appendix A.

4. Time integration

We apply a semi-implicit approach to Eqs. (18) and (14) that treats the streaming terms explicitly and the material-coupling terms implicitly. The P_N equations we are solving are highly nonlinear due to the presence of the T^4 term and the coupling to Eq. (14). Two common methods for resolving the nonlinearities are Newton's method and a linear Taylor-series expansion (equivalent to 1 partial Newton iteration). As it has been reported that the linear Taylor-series expansion performs well [21], we will use this technique to implicitly treat the nonlinearities. Before explaining our linearization, we will discuss our treatment of the streaming terms.

4.1. Predictor–corrector method

We use a predictor–corrector method that is equivalent to second-order accurate Runge–Kutta for the streaming operator [14]. The second-order Runge–Kutta method for a general ODE, $y'(t) = f(y(t), t)$, is given by

$$y^{n+1/2} = y^n + \frac{\Delta t}{2} f(y^n, n\Delta t), \tag{26}$$

$$y^{n+1} = y^n + \Delta t f(y^{n+1/2}, (n+1/2)\Delta t). \tag{27}$$

We will use this method for the streaming terms and backward Euler for the material coupling terms. The predictor step for Eq. (18) becomes

$$\mathbf{u}^{n+1/2} - \frac{c\Delta t}{2}\mathbf{q}(\mathbf{u}^{n+1/2}) = \mathbf{u}^n - \frac{c\Delta t}{2}\mathbf{A}\left.\frac{\mathrm{d}\mathbf{u}}{\mathrm{d}x}\right|_n, \tag{28}$$

$$e^{n+1/2} = e^n + \frac{\sigma\Delta t}{2}(\psi_0^{n+1/2} - ac(T^{n+1/2})^4), \tag{29}$$

where $\mathbf{u}^n = \mathbf{u}(x, n\Delta t)$. The corrector step is

$$\mathbf{u}^{n+1} - c\Delta t\mathbf{q}(\mathbf{u}^{n+1}) = \mathbf{u}^n - c\Delta t\mathbf{A}\left.\frac{\mathrm{d}\mathbf{u}}{\mathrm{d}x}\right|_{n+1/2}, \tag{30}$$

$$e^{n+1} = e^n + \sigma\Delta t(\psi_0^{n+1} - ac(T^{n+1})^4). \tag{31}$$

In this method the streaming terms are treated with second-order accuracy, while the collision and emission source terms' integration is first order. We have made this choice of schemes for robustness in the diffusion limit. We could treat the collision and emission terms with a second-order accurate implicit method such as Crank–Nicolson, however, such an approach can lead to oscillatory behavior if the time scale of these terms is not resolved [14].

4.2. Linearization of emission source

As mentioned at the outset of this section, we are going to treat the nonlinearities in the T^4 terms using the equivalent of one Newton iteration. To do this linearization, we require a third equation to linearize the $(T^{n+1})^4$ and $(T^{n+1/2})^4$ terms in Eqs. (28)–(31). A suitable choice is to expand $(T^{n+1})^4$ and e^{n+1} in a Taylor series about t^n,

$$e^{n+1} \approx e^n + C_v^n(T^{n+1} - T^n) + \mathrm{O}((T^{n+1} - T^n)^2), \tag{32}$$

$$(T^{n+1})^4 \approx (T^n)^4 + 4(T^n)^3(T^{n+1} - T^n) + \mathrm{O}((T^{n+1} - T^n)^2). \tag{33}$$

Using these equations along with Eq. (31) allows us to write,

$$(T^{n+1})^4 \approx \frac{ac(T^n)^4 + \sigma^n\beta^n\Delta t\psi_0^{n+1}}{ac(1 + \sigma^n\beta^n\Delta t)},$$

where

$$\beta^n = \frac{4ac(T^n)^3}{C_v^n}.$$

Substituting this expression into $\mathbf{q}$ from Eq. (30) yields

$$\mathbf{q}(\mathbf{u}^{n+1}) = \begin{pmatrix} f^n\sigma^n(ac(T^n)^4 - \psi_0^{n+1}) \\ -\sigma^n\psi_1^{n+1} \\ -\sigma^n\psi_2^{n+1} \\ \vdots \\ -\sigma^n\psi_N^{n+1} \end{pmatrix}, \tag{34}$$

where the factor f is given by

$$f^n = \frac{1}{1 + \sigma^n\beta^n\Delta t}. \tag{35}$$

Making the same substitution in Eq. (31) yields the following discretized, linear form of the material-energy equation,

$$e^{n+1} = e^n + f^n\sigma\Delta t(\psi_0^{n+1} - ac(T^{n+1})^4). \tag{36}$$

The linearization changes the coupling of the radiation equation to the material-energy equation. After linearizing, the radiation-transport equation can be solved for ψ_0^{n+1} because this equation now involves $(T^n)^4$ and does not receive implicit feedback from the material energy equation. Then ψ_0^{n+1} is used to evaluate e^{n+1}. Here we would like to note that our linearization scheme gives the same effective scattering and absorption terms equivalent to the Fleck and Cummings Implicit Monte Carlo approach to linearizing the blackbody source [2]. Specifically, the effective absorption is $f\sigma$ and the effective scattering is $(1 - f)\sigma$.

The linearized version of $q^{n+1/2}$ is formed in analogous fashion to that above. This expression is similar to Eq. (34), except the factor f^n is evaluated using $\Delta t \to \frac{1}{2}\Delta t$ and the radiation moments are evaluated at time level $n + 1/2$.

Our time-integration method does conserve energy. To demonstrate this point, we sum Eq. (30) for ψ_0 over all previous time steps to get

$$\frac{\psi_0^{n+1} - \psi^0}{c\Delta t} = -\sum_{i=0}^{n} \left.\frac{\mathrm{d}\psi_1}{\mathrm{d}x}\right|_{i+1/2} - \sum_{i=0}^{n} f^i \sigma^i (\psi_0^{i+1} - ac(T^i)^4). \tag{37}$$

Similarly, we sum Eq. (31) over all previous time steps:

$$\frac{e^{n+1} - e^0}{\Delta t} = \sum_{i=0}^{n} f^i \sigma^i (\psi_0^{i+1} - ac(T^i)^4). \tag{38}$$

Adding Eq. (37) to Eq. (38) and integrating over the spatial domain gives the statement of conservation,

$$\frac{1}{\Delta t}\int_{X^-}^{X^+} \mathrm{d}x\,[(E^{n+1} - E^0) + (e^{n+1} - e^0)] = \sum_{i=0}^{n} [F^{i+1/2}(X^-) - F^{i+1/2}(X^+)]. \tag{39}$$

This equation states that any change from the initial energy is due to energy entering or exiting through the boundary, as in the continuous equations.

4.3. Comparison with Klar's semi-implicit method

Our approach to treating the time variable involves integrating the streaming terms explicitly and the material interaction terms implicitly. Klar [16] and Klar and Unterreiter [17] investigated a semi-implicit scheme, which we shall refer to as the Klar method, that is similar to the one described above. The Klar method first splits the intensity into an even and odd component in μ, then integrates certain terms in the even and odd parts of the solution differently. For the P_N equations the method begins with a predictor step where the odd part of the solution is frozen and no material-interaction terms are considered:

$$\psi_0^{n+1/2} = \psi_0^n - c\Delta t \left.\frac{\mathrm{d}\psi_1}{\mathrm{d}x}\right|_n, \tag{40a}$$

$$\psi_l^{n+1/2} = \psi_l^n - c\Delta t\left(\frac{l}{2l+1}\left.\frac{\mathrm{d}\psi_{l-1}}{\mathrm{d}x}\right|_n + \frac{l+1}{2l+1}\left.\frac{\mathrm{d}\psi_{l+1}}{\mathrm{d}x}\right|_n\right), \quad l \text{ even}, \tag{40b}$$

$$\psi_l^{n+1/2} = \psi_l^n, \quad l \text{ odd}. \tag{40c}$$

This predictor step is then followed by a corrector step,

$$\psi_0^{n+1} = \psi_0^{n+1/2} - c\Delta t\sigma\left(\psi_0^{n+1} - ac(T^{n+1})^4\right), \tag{41a}$$

$$\psi_l^{n+1} = \psi_l^{n+1/2} - c\Delta t\sigma\psi_l^{n+1}, \quad l \text{ even}, \tag{41b}$$

$$\psi_l^{n+1} = \psi_l^{n+1/2} - c\Delta t\left(\frac{l}{2l+1}\left.\frac{\mathrm{d}\psi_{l-1}}{\mathrm{d}x}\right|_{n+1} + \frac{l+1}{2l+1}\left.\frac{\mathrm{d}\psi_{l+1}}{\mathrm{d}x}\right|_{n+1}\right) - c\Delta t\sigma\psi_l^{n+1}, \quad l \text{ odd}. \tag{41c}$$

In the context of the P_N equations, the Klar method is a first-order predictor–corrector approach. By treating the even and odd moments differently, the Klar method is robust in the diffusion limit, even when a finite difference method is used for the spatial discretization. Our semi-implicit scheme is second-order accurate for the streaming term. We treat the even and odd moments of the intensity in the same fashion and rely on our spatial discretization to give a robust diffusion limit (that is, we need to use discontinuous Galerkin finite elements to obtain a valid diffusion limit, whereas Klar's method is accurate in the diffusion limit with a finite difference scheme), as we will show later on in this study. In some sense it is easier to extend our approach to multi-dimensional problems because we need not generalize the notion of even and odd moments of the transport

equation to higher dimensions; such a generalization would necessitate a further splitting of the time-integration operator as there would be terms that are even or odd in the azimuthal and polar angles.

Despite the differences between our approach and that advocated by Klar, our method is surprisingly similar to a naive scheme rejected by Klar [16]. This simple time-integration scheme is

$$\mathbf{u}^{n+1} - c\Delta t\mathbf{q}(\mathbf{u}^{n+1}) = \mathbf{u}^n - c\Delta t\mathbf{A}\left.\frac{\mathrm{d}\mathbf{u}}{\mathrm{d}x}\right|_n. \tag{42}$$

This method uses forward Euler for the radiation streaming and backward Euler for the material interaction terms. Klar rejects this method because in the diffusion limit it limits to a discretization of the time-dependent diffusion equation where the spatial-derivative term is evaluated at the $n-1$ time step. This time-integration scheme has a smaller domain of stability and is less accurate than the standard explicit diffusion discretization. Our method is similar to that of Eq. (42) except that we use second-order accurate Runge–Kutta for the streaming term. Below, we show that by using second-order Runge–Kutta, we obtain a valid diffusion limit.

5. Spatial solution method

We will spatially discretize Eq. (18) using the discontinuous Galerkin (DG) finite element method [12,13]. We will then apply the time discretization that we detailed above to get the fully discrete system of equations that we solve numerically. We apply the DG method to Eq. (18) by first multiplying this equation by a basis function and integrating over a cell,

$$\frac{1}{c}\partial_t\int_{V_k} B_{k,i}\mathbf{u}\,\mathrm{d}x + \mathbf{A}[B_{k,i}\mathbf{u}] - \mathbf{A}\int_{V_k}\mathbf{u}\partial_x B_{k,i}\,\mathrm{d}x = \int_{V_k} B_{k,i}\mathbf{q}(\mathbf{u})\,\mathrm{d}x. \tag{43}$$

Here, $B_{k,i}(x)$ is the ith basis function of cell k and V_k is the "volume" (actually length, in this 1-D case) of the kth element. Also, $[\cdot] \equiv (\cdot)_{k+1/2} - (\cdot)_{k-1/2}$, where the subscripts "$_{k+1/2,k-1/2}$" refer to the right and left boundaries, respectively, of V_k. The unknown $\mathbf{u}(x,t)$ is expressed in terms of the basis functions as

$$\mathbf{u}(x,t) = \sum_{k=1}^{N_k}\sum_{j=1}^{N_p}\mathbf{u}_{k,j}(t)B_{k,j}(x), \tag{44}$$

where N_k is the number of spatial cells in the domain. In planar geometry $N_p = p+1$ with p equal to the polynomial order of the basis functions (for example, $N_p = 2$ for linear basis functions). Also, for the basis functions we use, each cell has N_p nodes, that is points in the cell were a basis function is unity. An example discretized mesh with linear basis functions is illustrated in Fig. 1.

If we substitute Eq. (44) into Eq. (43) and expand the $\mathbf{q}$ as in (44), then the result is N_p ordinary differential equations per cell in terms of the unknowns $\mathbf{u}_{k,j}(t)$, $1 \leqslant j \leqslant N_p$. Specifically, we obtain for a particular cell

$$\frac{1}{c}M_{k,i,j}\frac{\mathrm{d}}{\mathrm{d}t}\mathbf{u}_{k,j} + \mathbf{A}[B_i\mathbf{u}] - K_{k,i,j}\mathbf{A}\mathbf{u}_{k,j} = M_{k,i,j}\mathbf{q}(\mathbf{u}_{k,j}), \quad 1 \leqslant i \leqslant N_p, \tag{45}$$

where

$$M_{k,i,j} = \int_{V_k} B_{k,i}B_{k,j}\,\mathrm{d}x, \quad K_{k,i,j} = \int_{V_k} B_{k,j}\partial_x B_{k,i}\,\mathrm{d}x, \tag{46}$$

and we sum over the repeated j subscript.

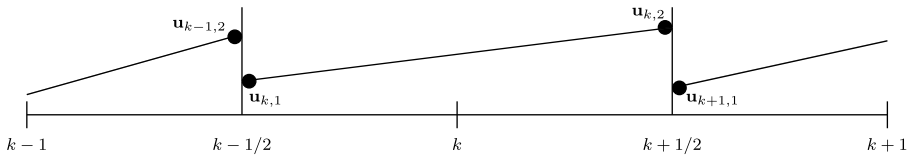

Fig. 1. Discretized planar-geometry mesh. The k indices refer to a particular cell, while the second subscript refers to a particular node within that cell. Each cell has two nodes in the case of linear basis functions.

Generally, the expansion in Eq. (44) is discontinuous across cell boundaries. To ensure conservation, the same value for $\mathbf{A}\mathbf{u}_{k+1/2}$ must be used for cell k and $k+1$. Let $\mathbf{u}_{k+1/2,L}$ be the boundary value from cell k and $\mathbf{u}_{k+1/2,R}$ the value from cell $k+1$. Then we "upwind" [20] to find $\mathbf{A}\mathbf{u}_{k+1/2}$:

$$\mathbf{A}\mathbf{u}_{k+1/2} = \mathbf{A}\bar{\mathbf{u}}_{k+1/2} - \frac{1}{2}|\mathbf{A}|\Delta\mathbf{u}_{k+1/2} \tag{47}$$

where

$$\bar{\mathbf{u}}_{k+1/2} = \frac{1}{2}(\mathbf{u}_{k+1/2,L} + \mathbf{u}_{k+1/2,R}), \tag{48}$$

$$\Delta\mathbf{u}_{k+1/2} = \mathbf{u}_{k+1/2,R} - \mathbf{u}_{k+1/2,L}, \tag{49}$$

$$|\mathbf{A}| = \mathbf{R}|\mathbf{\Lambda}|\mathbf{R}^{-1}. \tag{50}$$

This way of defining $\mathbf{A}\mathbf{u}_{k+1/2}$ upwinds in the sense that positive eigenvalues move information from the left to the right ($\mathbf{u}_{k,2} \to \mathbf{u}_{k+1/2}$) and negative eigenvalues move information from the right to the left ($\mathbf{u}_{k,1} \to \mathbf{u}_{k-1/2}$). For the planar-geometry equations this upwinding makes our discrete P_N equations equivalent to the DG method for the discrete-ordinates equations with Gaussian quadrature.

As an example of our upwinding, for P_1 we obtain

$$\mathbf{A}\mathbf{u}_{k+1/2} = \begin{pmatrix} \bar{\psi}_1 \\ \frac{1}{3}\bar{\psi}_0 \end{pmatrix}_{k+1/2} - \frac{1}{2\sqrt{3}}\begin{pmatrix} \Delta\psi_0 \\ \Delta\psi_1 \end{pmatrix}_{k+1/2}. \tag{51}$$

5.1. Linear basis functions

In this subsection, we develop the method for linear basis functions. There are two basis functions ($N_p = 2$) that are defined on a generic cell $x_k - \Delta x_k/2 \leqslant x \leqslant x_k + \Delta x_k/2$, where x_k is the cell center and Δx_k is the cell size, as

$$B_{1,k}(x) = \frac{x_k + \frac{\Delta x_k}{2} - x}{\Delta x_k}, \quad B_{2,k}(x) = \frac{x - x_k + \frac{\Delta x_k}{2}}{\Delta x_k}. \tag{52}$$

With this choice, Eq. (44) gives that $\mathbf{u}_{k,1}(t)$ is the value on the left side of the cell, while $\mathbf{u}_{k,2}(t)$ is the value on the right side. Eq. (45) then becomes

$$\frac{1}{c}M_{k,i,j}\frac{\mathrm{d}}{\mathrm{d}t}\mathbf{u}_{k,j} + \delta_{i,2}(\mathbf{A}\mathbf{u})_{k+1/2} - \delta_{i,1}(\mathbf{A}\mathbf{u})_{k-1/2} - K_{k,i,j}\mathbf{A}\mathbf{u}_{k,j} = M_{k,i,j}\mathbf{q}(\mathbf{u}_{k,j}), \quad i = 1,2 \tag{53}$$

with

$$\mathbf{M}_k = \frac{\Delta x_k}{6}\begin{pmatrix} 2 & 1 \\ 1 & 2 \end{pmatrix}, \quad \mathbf{K}_k = \frac{1}{2}\begin{pmatrix} -1 & -1 \\ 1 & 1 \end{pmatrix}, \tag{54}$$

$$\delta_{i,1} = \begin{pmatrix} 1 \\ 0 \end{pmatrix}, \quad \delta_{i,2} = \begin{pmatrix} 0 \\ 1 \end{pmatrix}. \tag{55}$$

The matrix $\mathbf{M}$ is known as mass matrix. Multiplying through by $\mathbf{M}^{-1}$ gives

$$\frac{1}{c}\frac{\mathrm{d}}{\mathrm{d}t}\mathbf{u}_{k,1} + \frac{-2(\mathbf{A}\mathbf{u})_{k+1/2} - 4(\mathbf{A}\mathbf{u})_{k-1/2} + 3\mathbf{A}(\mathbf{u}_{k,1} + \mathbf{u}_{k,2})}{\Delta x_k} = \mathbf{q}(\mathbf{u}_{k,1}), \tag{56}$$

$$\frac{1}{c}\frac{\mathrm{d}}{\mathrm{d}t}\mathbf{u}_{k,2} + \frac{2(\mathbf{A}\mathbf{u})_{k-1/2} + 4(\mathbf{A}\mathbf{u})_{k+1/2} - 3\mathbf{A}(\mathbf{u}_{k,1} + \mathbf{u}_{k,2})}{\Delta x_k} = \mathbf{q}(\mathbf{u}_{k,2}). \tag{57}$$

Adding these equations gives the correct balance equation,

$$\frac{1}{2c}\frac{\mathrm{d}}{\mathrm{d}t}(\mathbf{u}_{k,1} + \mathbf{u}_{k,2}) + \frac{(\mathbf{A}\mathbf{u})_{k+1/2} - (\mathbf{A}\mathbf{u})_{k-1/2}}{\Delta x_k} = \frac{1}{2}(\mathbf{q}(\mathbf{u}_{k,1}) + \mathbf{q}(\mathbf{u}_{k,2})), \tag{58}$$

a statement that the time evolution of the average value of $\mathbf{u}$ in a cell is the result of the net inflow plus the source. Furthermore, this is a conservative balance equation. We now have enough information to solve Eq. (45).

We also apply the expansion in Eq. (44) to T^4 and e in the material-energy equation to get

$$\frac{\mathrm{d}}{\mathrm{d}t}e_{k,j} = \sigma(\psi_{0,k,j} - ac(T_{k,j})^4), \quad j = 1, 2. \tag{59}$$

The fully discrete equations are obtained by applying the time discretization presented in Section 4 to Eqs. (56) and (57) to get

Predictor step

$$\frac{1}{c}\frac{\mathbf{u}_{k,1}^{n+1/2} + \mathbf{u}_{k,1}^{n}}{\Delta t/2} + \frac{-2(\mathbf{Au})_{k+1/2}^{n} - 4(\mathbf{Au})_{k-1/2}^{n} + 3\mathbf{A}(\mathbf{u}_{k,1}^{n} + \mathbf{u}_{k,2}^{n})}{\Delta x_k} = \mathbf{q}(\mathbf{u}_{k,1}^{n+1/2}), \tag{60a}$$

$$\frac{1}{c}\frac{\mathbf{u}_{k,2}^{n+1/2} + \mathbf{u}_{k,2}^{n}}{\Delta t/2} + \frac{2(\mathbf{Au})_{k-1/2}^{n} + 4(\mathbf{Au})_{k+1/2}^{n} - 3\mathbf{A}(\mathbf{u}_{k,1}^{n} + \mathbf{u}_{k,2}^{n})}{\Delta x_k} = \mathbf{q}(\mathbf{u}_{k,2}^{n+1/2}). \tag{60b}$$

Corrector step

$$\frac{1}{c}\frac{\mathbf{u}_{k,1}^{n+1} + \mathbf{u}_{k,1}^{n}}{\Delta t} + \frac{-2(\mathbf{Au})_{k+1/2}^{n+1/2} - 4(\mathbf{Au})_{k-1/2}^{n+1/2} + 3\mathbf{A}(\mathbf{u}_{k,1}^{n+1/2} + \mathbf{u}_{k,2}^{n+1/2})}{\Delta x_k} = \mathbf{q}(\mathbf{u}_{k,1}^{n+1}), \tag{61a}$$

$$\frac{1}{c}\frac{\mathbf{u}_{k,2}^{n+1} + \mathbf{u}_{k,2}^{n}}{\Delta t} + \frac{2(\mathbf{Au})_{k-1/2}^{n+1/2} + 4(\mathbf{Au})_{k+1/2}^{n+1/2} - 3\mathbf{A}(\mathbf{u}_{k,1}^{n+1/2} + \mathbf{u}_{k,2}^{n+1/2})}{\Delta x_k} = \mathbf{q}(\mathbf{u}_{k,2}^{n+1}). \tag{61b}$$

These equations will be governed by a CFL limit for the time step size. This time-step limit is [13]

$$\frac{c\Delta t}{\Delta x} \leqslant \frac{1}{3}. \tag{62}$$

Satisfying this CFL condition will give a stable update in any regime. As we shall see though, in diffusive problems there is a less restrictive time step limit.

6. Slope limiting

The linear discontinuous finite element discretization described above is a linear, second-order accurate spatial discretization. Such a linear, second-order scheme for a hyperbolic system like the P_N equations will allow the creation of artificial oscillations in the solution: this fact is a result of Godunov's Theorem [20]. To prevent oscillations, we will use a slope-limiting method [13]. Alternatively, we could lump the mass matrix [22]; this process would add numerical dissipation to damp oscillations. However, lumping does not suppress all oscillations, and the lumped equations are less accurate than their unlumped counterparts.

After each step (either predictor or corrector) we first compute an average in each cell,

$$\bar{\mathbf{u}}_k = \frac{1}{2}(\mathbf{u}_{k,2} + \mathbf{u}_{k,1}), \tag{63}$$

and then change the node values for the cell to be

$$\tilde{\mathbf{u}}_{k,1} = \bar{\mathbf{u}}_k - \frac{\mathbf{s}_k}{2} \quad \text{and} \quad \tilde{\mathbf{u}}_{k,2} = \bar{\mathbf{u}}_k + \frac{\mathbf{s}_k}{2}.$$

Here, the slope is calculated on an cell-by-cell and moment-by-moment basis using

$$s_{l,k} = \mathcal{M}(u_{l,k,2} - u_{l,k,1}, \alpha(\bar{u}_{l,k} - \bar{u}_{l,k-1}), \alpha(\bar{u}_{l,k+1} - \bar{u}_{l,k})), \tag{64}$$

for $\alpha \in [0, 2]$, and $\mathcal{M}$, the minmod function, given by

$$\mathcal{M}(a, b, c) = \begin{cases} \min(a, b, c) & \operatorname{sign}(a) = \operatorname{sign}(b) = \operatorname{sign}(c), \\ 0 & \text{otherwise.} \end{cases} \tag{65}$$

Choosing $\alpha = 0$ causes the cell-edge values to equal their average; this method is the first-order upwind, Godunov scheme. In the transport literature, this method is also known as the "step" scheme because the values in each cell are flat and discontinuous at a cell interface. The step scheme is known to not be accurate in the diffusion limit [23] and will not be considered further here. With $\alpha = 1$ the limiter is identical to the minmod limiter [20]. When $\alpha = 2$ we have the monotonized center or double minmod limiter [24]. In this case the edge values in cell k are no bigger than the average value of either neighbor's average value. Unless otherwise stated, we will use $\alpha = 2$ for the remainder of our study.

7. Boundary conditions

At problem boundaries we must specify the incoming intensity. Brunner and Holloway studied different boundary conditions for upwind discretizations of the P_N equations and determined that the Mark boundary condition implemented with ghost cells yields a good combination of performance and straightforward implementation [25]. Later, it was shown that it is possible to specify a reflecting boundary using ghost cells [8]. To specify a boundary condition using ghost cells, cells are placed just outside the physical system boundary where we specify the moments of the incoming intensities. This process treats the system boundary in an identical manner as an interface between interior cells. This treatment is appropriate because our upwind discretization moves information in the appropriate directions – in this case moving only from the ghost cell into the physical system.

8. The asymptotic limit of the discrete equations

We now present an analysis of our numerical method in the equilibrium diffusion limit [26]. To analyze the behavior of the method in this limit, we will scale different terms in the equations using a small parameter $\epsilon \ll 1$ and constant Δt. The diffusion limit corresponds to the situation where the mean-free time of a photon is $O(\epsilon^2)$ compared with the time scale over which $\mathbf{u}$ and e vary by $O(1)$, and the mean-free path is $O(\epsilon)$ compared with the length scale over which $\mathbf{u}$ and e vary by $O(1)$. To achieve this situation we will scale the absorption opacity by ϵ^{-1}, the heat capacity by ϵ, and the speed of light by ϵ^{-1}. For consistency the internal energy is also scaled by ϵ. The time step size, Δt, is considered to be an $O(1)$ quantity because we are interested in the case where we approach the diffusion limit with a fixed time step. The scaling of these parameters was introduced in Ref. [26] and has been used several times in the past [27–29] to analyze radiation transport methods. In the equilibrium diffusion limit, to leading order in ϵ the thermal radiative-transfer system is replaced by a diffusion equation for the material temperature,

$$\frac{\partial e^{(0)}}{\partial t} + a\frac{\partial}{\partial t}(T^{(0)})^4 = \frac{\partial}{\partial x}\frac{ac}{3\sigma}\frac{\partial}{\partial x}(T^{(0)})^4, \tag{66}$$

and the zeroth angular moment (proportional to the radiation energy density) is described by a Planck function at the local temperature,

$$\psi_0^{(0)} = ac(T^{(0)})^4, \tag{67}$$

and to first order in ϵ the first angular moment of the radiation intensity is given by Fick's law,

$$F^{(1)} = \psi_1^{(1)} = -\frac{ac}{3\sigma}\frac{\partial}{\partial x}\left(T^{(0)}\right)^4. \tag{68}$$

In Eqs. (66)–(68) the superscripts indicate terms in an asymptotic series (see Eq. (71)).

For a numerical method for thermal radiative transfer to be "asymptotic preserving" (also referred to as having the diffusion limit), the method must give a valid discretization of Eq. (66) and enforce the condition in Eq. (67). When a method does preserve this limit, it is possible to use cells that are optically thick (i.e., many mean-free paths thick) and still obtain accurate solutions. Methods not having a valid diffusion limit will give erroneous results when the mean-free path is not resolved, even when the spatial variation of the solution is resolved. In realistic thermal radiative-transfer problems, resolving the mean-free path requires prohibitively small cell sizes and is not practical.

In the remainder of this section, we will examine our method in the asymptotic limit away from boundary and initial layers to see if the method gives a valid discretization of Eq. (66). In the interest of clarity we will restrict our analysis to the situation of constant σ and C_v. This analysis will be similar to that of Larsen and Morel [30] for the linear discontinuous Galerkin method applied to the planar-geometry S_N equations in steady state. This similarity is due to the fact that, in slab geometry, the P_N equations are equivalent to S_N with Gauss–Legendre quadrature [19]. While there are similarities in the planar-geometry case, we believe this analysis will be useful for future work with the multidimensional P_N equations. We do not include the effects of the slope limiter in our analysis because of its non-smooth character. Later, the effect of the slope limiter will be included in numerical results.

We begin by scaling the radiation equations for the corrector step,

$$\frac{\epsilon}{c}\frac{\mathbf{u}_{k,1}^{n+1}-\mathbf{u}_{k,1}^{n}}{\Delta t}+\frac{-2\mathbf{A}\mathbf{u}_{k+1/2}^{n+1/2}-4\mathbf{A}\mathbf{u}_{k-1/2}^{n+1/2}+3\mathbf{A}(\mathbf{u}_{k,1}^{n+1/2}+\mathbf{u}_{k,2}^{n+1/2})}{\Delta x} = \begin{cases} \frac{\epsilon}{\beta_{k,1}^{n}\Delta t}(ac(T_{k,1}^{n})^4-\psi_{0,k,1}^{n+1})+\mathrm{O}(\epsilon^3) & l=0, \\ -\epsilon^{-1}\sigma\psi_{l,k,1}^{n+1} & l\neq 0. \end{cases} \tag{69a}$$

$$\frac{\epsilon}{c}\frac{\mathbf{u}_{k,2}^{n+1}-\mathbf{u}_{k,2}^{n}}{\Delta t}+\frac{4\mathbf{A}\mathbf{u}_{k+1/2}^{n+1/2}+2\mathbf{A}\mathbf{u}_{k-1/2}^{n+1/2}-3\mathbf{A}(\mathbf{u}_{k,1}^{n+1/2}+\mathbf{u}_{k,2}^{n+1/2})}{\Delta x} = \begin{cases} \frac{\epsilon}{\beta_{k,2}^{n}\Delta t}\left(ac(T_{k,2}^{n})^4-\psi_{0,k,2}^{n+1}\right)+\mathrm{O}(\epsilon^3) & l=0, \\ -\epsilon^{-1}\sigma\psi_{l,k,2}^{n+1} & l\neq 0. \end{cases} \tag{69b}$$

In the $l=0$ equation we have used the fact that under our scaling [27]

$$f\sigma\rightarrow\frac{\epsilon^{-1}\sigma}{1+\epsilon^{-2}\beta\sigma\Delta t}=\frac{\epsilon}{\beta\Delta t}+\mathrm{O}(\epsilon^3).$$

The equations for the predictor step are scaled in an identical way to Eqs. (69). The discrete material energy equation is

$$e_{k,j}^{n+1}=e_{k,j}^{n}+\beta^{-1}(\psi_{0,k,j}^{n+1}-ac(T_{k,j}^{n})^4). \tag{70}$$

We now postulate an expansion of $\mathbf{u}$, e, and T^4 in ϵ,

$$(\cdot)=\sum_{k=0}^{\infty}\epsilon^m(\cdot)^{(m)}, \tag{71}$$

and substitute this expansion into the scaled P_N equations. The equations at $\mathrm{O}(\epsilon^{-1})$ are

$$\psi_{l,k,j}^{(0),n+1/2}=\psi_{l,k,j}^{(0),n+1}=0,\quad l\neq 0 \text{ and } j=1,2. \tag{72}$$

Therefore, all the moments greater than zero vanish to leading order. At $\mathrm{O}(1)$ the material energy equations tell us that the leading order zeroth-moment is in equilibrium with the linearized blackbody source, i.e.,

$$\psi_{0,k,j}^{(0),n+1}=ac(T_{k,j}^{(0),n})^4+4ac(T_{k,j}^{(0),n})^3(T_{k,j}^{(0),n+1}-T_{k,j}^{(0),n}),\quad j=1,2. \tag{73}$$

We note that the right side of Eq. (73) is a second-order-in-Δt approximation to $ac(T^{n+1})^4$ so that

$$\psi_{0,k,j}^{(0),n+1}=ac(T_{k,j}^{(0),n+1})^4+\mathrm{O}(\Delta t^2). \tag{74}$$

The $l=0$ radiation equations for the corrector step at $\mathrm{O}(1)$ are

$$\frac{-2\mathbf{A}_0\mathbf{u}_{k+1/2}^{(0),n+1/2}-4\mathbf{A}_0\mathbf{u}_{k-1/2}^{(0),n+1/2}+3\mathbf{A}_0(\mathbf{u}_{k,1}^{(0),n+1/2}+\mathbf{u}_{k,2}^{(0),n+1/2})}{\Delta x}=0, \tag{75a}$$

$$\frac{4\mathbf{A}_0\mathbf{u}_{k+1/2}^{(0),n+1/2}+2\mathbf{A}_0\mathbf{u}_{k-1/2}^{(0),n+1/2}-3\mathbf{A}_0(\mathbf{u}_{k,1}^{(0),n+1/2}+\mathbf{u}_{k,2}^{(0),n+1/2})}{\Delta x}=0. \tag{75b}$$

The predictor step equations are identical except $n+1/2 \rightarrow n$. In the above equations we have denoted the zeroth matrix row by the subscript 0. These equations can be simplified by using the structure of the matrix $\mathbf{A}$. This matrix has the form

$$\mathbf{A} = \begin{pmatrix} 0 & 1 & 0 & \dots & & & & \\ \frac{1}{3} & 0 & \frac{2}{3} & 0 & \dots & & & \\ 0 & \frac{2}{5} & 0 & \frac{3}{5} & 0 & \dots & & \\ & & & \frac{l}{2l+1} & 0 & \frac{l+1}{2l+1} & 0 & \dots \\ & & & & \ddots & \ddots & \ddots & 0 & \dots \end{pmatrix}. \tag{76}$$

Thus, the product of $\mathbf{A}$ and the leading order vector of intensity moments is

$$\mathbf{A}\mathbf{u}^{(0)} = \begin{pmatrix} 0 \\ \frac{1}{3}\psi_0^{(0)} \\ 0 \\ \vdots \end{pmatrix} \tag{77}$$

The element-by-element structure of $|\mathbf{A}|$ is given in the following expression:

$$|\mathbf{A}|_{i,j} = \begin{cases} 0 & \mathrm{mod}(i,2) \neq \mathrm{mod}(j,2), \\ a_{i,j} & \text{otherwise}, \end{cases} \tag{78}$$

for some non-zero $a_{i,j}$. Using the structure of $\mathbf{A}\mathbf{u}^{(0)}$ and $|\mathbf{A}|_{i,j}$, Eqs. (75a) and (75b) become

$$-|\mathbf{A}|_{0,0}(\psi_{0,k+1,1}^{(0),n+1/2} - \psi_{0,k,2}^{(0),n+1/2}) - 2|\mathbf{A}|_{0,0}(\psi_{0,k,1}^{(0),n+1/2} - \psi_{0,k-1,2}^{(0),n+1/2}) = 0, \tag{79a}$$

$$2|\mathbf{A}|_{0,0}(\psi_{0,k+1,1}^{(0),n+1/2} - \psi_{0,k,2}^{(0),n+1/2}) + |\mathbf{A}|_{0,0}(\psi_{0,k,1}^{(0),n+1/2} - \psi_{0,k-1,2}^{(0),n+1/2}) = 0. \tag{79b}$$

These equations are a linear system of homogeneous equations with full rank, therefore, the solution space to this system is zero dimensional and only contains the zero vector [31]. This fact makes $\mathbf{u}^{(0)}$ continuous at a cell edge. In this asymptotic scaling the discontinuous finite element method becomes a continuous finite element method to leading order,

$$\mathbf{u}_{k,2}^{(0),n} = \mathbf{u}_{k+1,1}^{(0),n}, \tag{80a}$$

$$\mathbf{u}_{k,2}^{(0),n+1/2} = \mathbf{u}_{k+1,1}^{(0),n+1/2}. \tag{80b}$$

The higher moment equations ($l > 0$) for the corrector step at O(1) are

$$\frac{-2\mathbf{A}_l\mathbf{u}_{k+1/2}^{(0),n+1/2} - 4\mathbf{A}_l\mathbf{u}_{k-1/2}^{(0),n+1/2} + 3\mathbf{A}_l(\mathbf{u}_{k,1}^{(0),n+1/2} + \mathbf{u}_{k,2}^{(0),n+1/2})}{\Delta x} = -\sigma\psi_{l,k,1}^{(1),n+1}, \tag{81a}$$

$$\frac{4\mathbf{A}_l\mathbf{u}_{k+1/2}^{(0),n+1/2} + 2\mathbf{A}_l\mathbf{u}_{k-1/2}^{(0),n+1/2} - 3\mathbf{A}_l(\mathbf{u}_{k,1}^{(0),n+1/2} + \mathbf{u}_{k,2}^{(0),n+1/2})}{\Delta x} = -\sigma\psi_{l,k,2}^{(1),n+1}. \tag{81b}$$

Once again using the structure of the $\mathbf{A}$ and $|\mathbf{A}|$, these equations simplify to

$$\psi_{1,k,j}^{(1),n+1} = -\frac{\psi_{0,k,2}^{(0),n+1/2} - \psi_{0,k,1}^{(0),n+1/2}}{3\sigma\Delta x}, \tag{82a}$$

$$\psi_{l,k,j}^{(1),n+1} = 0, \quad l > 1, \tag{82b}$$

for $j = 1, 2$. Similarly, the predictor step equations give

$$\psi_{1,k,j}^{(1),n+1/2} = -\frac{\psi_{0,k,2}^{(0),n} - \psi_{0,k,1}^{(0),n}}{3\sigma\Delta x}, \tag{83a}$$

$$\psi_{l,k,j}^{(1),n+1/2} = 0, \quad l > 1, \tag{83b}$$

for $j = 1, 2$.

The $l = 0$ equations for the corrector step to $O(\epsilon)$ are

$$\frac{1}{c}\frac{\psi_{0,k,1}^{(0),n+1} - \psi_{0,k,1}^{(0),n}}{\Delta t} + \frac{-2\mathbf{A}_0\mathbf{u}_{k+1/2}^{(1),n+1/2} - 4\mathbf{A}_0\mathbf{u}_{k-1/2}^{(1),n+1/2} + 3\mathbf{A}_0(\mathbf{u}_{k,1}^{(1),n+1/2} + \mathbf{u}_{k,2}^{(1),n+1/2})}{\Delta x} = \frac{1}{\beta_{k,1}^n \Delta t}(ac(T_{k,1}^{(0),n})^4 - \psi_{0,k,1}^{(0),n+1}), \tag{84a}$$

$$\frac{1}{c}\frac{\psi_{0,k,2}^{(0),n+1} - \psi_{0,k,2}^{(0),n}}{\Delta t} + \frac{4\mathbf{A}_0\mathbf{u}_{k+1/2}^{(1),n+1/2} + 2\mathbf{A}_0\mathbf{u}_{k-1/2}^{(1),n+1/2} - 3\mathbf{A}_0(\mathbf{u}_{k,1}^{(1),n+1/2} + \mathbf{u}_{k,2}^{(1),n+1/2})}{\Delta x} = \frac{1}{\beta_{k,2}^n \Delta t}(ac(T_{k,2}^{(0),n})^4 - \psi_{0,k,2}^{(0),n+1}). \tag{84b}$$

To proceed we will define a cell average of $\mathbf{u}$ or e, $\bar{(\cdot)}_k$, as

$$\bar{(\cdot)}_k = \frac{1}{2}((\cdot)_{k,1} + (\cdot)_{k,2}), \tag{85}$$

and the difference across a cell, $\hat{\mathbf{u}}_k$, as

$$\hat{(\cdot)}_k = \frac{1}{2}((\cdot)_{k,2} - (\cdot)_{k,1}). \tag{86}$$

We can manipulate Eqs. (84) to give expressions involving $\bar{\mathbf{u}}_k$ and $\hat{\mathbf{u}}_k$:

$$\frac{\mathbf{A}_0\mathbf{u}_{k+1/2}^{(1),n+1/2} - \mathbf{A}_0\mathbf{u}_{k-1/2}^{(1),n+1/2}}{\Delta x} = -\frac{\bar{e}_k^{(0),n+1} - \bar{e}_k^{(0),n}}{\Delta t} - \frac{1}{c}\frac{\bar{\psi}_{0,k}^{(0),n+1} - \bar{\psi}_{0,k}^{(0),n}}{\Delta t}, \tag{87a}$$

$$\frac{\mathbf{A}_0\mathbf{u}_{k+1/2}^{(1),n+1/2} + \mathbf{A}_0\mathbf{u}_{k-1/2}^{(1),n+1/2}}{\Delta x} = \frac{\mathbf{A}_0\bar{\mathbf{u}}_k^{(1),n+1/2}}{\Delta x} - \frac{\hat{e}_k^{(0),n+1} - \hat{e}_k^{(0),n}}{3\Delta t} - \frac{1}{3c}\frac{\hat{\psi}_{0,k}^{(0),n+1} - \hat{\psi}_{0,k}^{(0),n}}{\Delta t}, \tag{87b}$$

where we have used Eq. (70) to replace the material interaction term with the temporal difference of the internal energy. By adding Eq. (87a) over cell k and $k+1$ we get

$$\frac{\mathbf{A}_0\mathbf{u}_{k+3/2}^{(1),n+1/2} - \mathbf{A}_0\mathbf{u}_{k-1/2}^{(1),n+1/2}}{\Delta x} = -\frac{\bar{e}_{k+1}^{(0),n+1} + \bar{e}_k^{(0),n+1} - \bar{e}_{k+1}^{(0),n} - \bar{e}_k^{(0),n}}{\Delta t} - \frac{1}{c}\frac{\bar{\psi}_{0,k+1}^{(0),n+1} + \bar{\psi}_{0,k}^{(0),n+1} - \bar{\psi}_{0,k+1}^{(0),n} - \bar{\psi}_{0,k}^{(0),n}}{\Delta t}. \tag{88}$$

Next we subtract Eq. (87b) for cell k from that equation for $k+1$ to get

$$\frac{\mathbf{A}_0\mathbf{u}_{k+3/2}^{(1),n+1/2} - \mathbf{A}_0\mathbf{u}_{k-1/2}^{(1),n+1/2}}{\Delta x} = \frac{\mathbf{A}_0(\bar{\mathbf{u}}_{k+1}^{(1),n+1/2} - \bar{\mathbf{u}}_k^{(1),n+1/2})}{\Delta x} - \frac{\hat{e}_{k+1}^{(0),n+1} - \hat{e}_k^{(0),n+1} - \hat{e}_{k+1}^{(0),n} + \hat{e}_k^{(0),n}}{3\Delta t} + \frac{1}{3c}\frac{\hat{\psi}_{0,k+1}^{(0),n+1} - \hat{\psi}_{0,k}^{(0),n+1} - \hat{\psi}_{0,k+1}^{(0),n} + \hat{\psi}_{0,k}^{(0),n}}{\Delta t}. \tag{89}$$

Upon equating Eqs. (88) and (89), we get the equation

$$\frac{-\mathbf{A}_0(\bar{\mathbf{u}}_{k+1}^{(1),n+1/2} - \bar{\mathbf{u}}_k^{(1),n+1/2})}{\Delta x} = \frac{(\bar{e}_{k+1}^{(0),n+1} - \frac{1}{3}\hat{e}_{k+1}^{(0),n+1}) + (\bar{e}_{k+1}^{(0),n+1} + \frac{1}{3}\hat{e}_k^{(0),n+1}) - (\bar{e}_{k+1}^{(0),n} - \frac{1}{3}\hat{e}_{k+1}^{(0),n}) - (\bar{e}_k^{(0),n} + \frac{1}{3}\hat{e}_k^{(0),n})}{\Delta t} + \frac{1}{c}\frac{(\bar{\psi}_{0,k+1}^{(0),n+1} - \frac{1}{3}\hat{\psi}_{0,k+1}^{(0),n+1}) + (\bar{\psi}_{0,k}^{(0),n+1} + \frac{1}{3}\hat{\psi}_{0,k}^{(0),n+1}) - (\bar{\psi}_{0,k+1}^{(0),n} - \frac{1}{3}\hat{\psi}_{0,k+1}^{(0),n}) - (\bar{\psi}_{0,k}^{(0),n} - \frac{1}{3}\hat{\psi}_{0,k}^{(0),n})}{\Delta t}. \tag{90}$$

To get a diffusion equation we use a relation that results from our discrete version of Fick's law, Eq. (83a),

$$\mathbf{A}_0\mathbf{u}_{k,j}^{(1),n+1/2} = \psi_{1,k,j}^{(1),n+1/2} = -\frac{1}{3\sigma\Delta x}(\psi_{0,k,2}^{(0),n} - \psi_{0,k,1}^{(0),n}). \tag{91}$$

Using this relation we get the equation

$$\begin{aligned}
&\frac{1}{3\sigma\Delta x^2}(\psi^{(0),n}_{0,k+1,2} - 2\psi^{(0),n}_{0,k,2} + \psi^{(0),n}_{0,k,1}) \\
&\quad = \frac{(\bar{e}^{(0),n+1}_{k+1} - \frac{1}{3}\hat{e}^{(0),n+1}_{k+1}) + (\bar{e}^{(0),n+1}_{k+1} + \frac{1}{3}\hat{e}^{(0),n+1}_{k}) - (\bar{e}^{(0),n}_{k+1} - \frac{1}{3}\hat{e}^{(0),n}_{k+1}) - (\bar{e}^{(0),n}_{k} + \frac{1}{3}\hat{e}^{(0),n}_{k})}{\Delta t} \\
&\qquad - \frac{1}{c}\frac{(\bar{\psi}^{(0),n+1}_{0,k+1} - \frac{1}{3}\hat{\psi}^{(0),n+1}_{0,k+1}) + (\bar{\psi}^{(0),n+1}_{0,k} + \frac{1}{3}\hat{\psi}^{(0),n+1}_{0,k}) - (\bar{\psi}^{(0),n}_{0,k+1} - \frac{1}{3}\hat{\psi}^{(0),n}_{0,k+1}) - (\bar{\psi}^{(0),n}_{0,k} - \frac{1}{3}\hat{\psi}^{(0),n}_{0,k})}{\Delta t}.
\end{aligned} \tag{92}$$

To simplify this equation we will define a weighted average, $\breve{(\cdot)}$,

$$\breve{(\cdot)}_{k,2} \equiv \left\{ \bar{(\cdot)}_{0,k+1} - \frac{1}{3}\hat{(\cdot)}_{0,k+1} + \left(\bar{(\cdot)}_{0,k} + \frac{1}{3}\hat{(\cdot)}_{0,k}\right) \right\} = \frac{1}{6}(\cdot)_{0,k+1,2} + \frac{2}{3}(\cdot)_{0,k,2} + \frac{1}{6}(\cdot)_{0,k,1}. \tag{93}$$

Using Eq. (74) and the weighted average definition makes Eq. (92) to $O(\Delta t^2)$

$$ac\frac{\left(T^{(0),n}_{k+1,2}\right)^4 - 2(T^{(0),n}_{k,2})^4 + (T^{(0),n}_{k,1})^4}{3\sigma\Delta x^2} = \frac{\breve{e}^{(0),n+1}_{k,2} - \breve{e}^{(0),n}_{k,2}}{\Delta t} + a\frac{(\breve{T}^{(0),n+1}_{k,2})^4 - (\breve{T}^{(0),n}_{k,2})^4}{\Delta t}. \tag{94}$$

This equation is a valid discretization of the equilibrium diffusion equation, Eq. (66), and thus our linear discontinuous Galerkin P_N method preserves the asymptotic diffusion limit. We note that in this limit the predictor and corrector steps are decoupled in the sense that the $n+1$ time-level quantities do not depend on the $n+1/2$ time-level quantities, and the time discretization becomes equivalent to forward Euler.

The above asymptotic analysis can also be performed for the case where Δt is a $O(\epsilon)$ quantity, the so-called intermediate limit [23]. In this limit our method limits to the same discretization of the equilibrium diffusion equations as Eq. (94).

8.1. Stability analysis of the discrete asymptotic limit

In the diffusion limit the predictor–corrector method transitions to the forward Euler method. To examine the stability of the discrete diffusion equation, Eq. (94), we will perform a von Neumann analysis on a linear version of this equation (for an example of this analysis on finite difference methods, see [32]),

$$\frac{E^n_{k+1,2} - 2E^n_{k,2} + E^n_{k,1}}{3\sigma\Delta x} = \frac{1}{c}\frac{\breve{E}^{n+1}_{k,2} - \breve{E}^{n}_{k,2}}{\Delta t}. \tag{95}$$

We now decompose the solution into individual Fourier modes

$$E^n_{k,1} = \alpha_m(n\Delta t)A_m \exp(\mathrm{i}m(k-1)\Delta x), \tag{96a}$$

$$E^n_{k,2} = \alpha_m(n\Delta t)A_m \exp(\mathrm{i}mk\Delta x), \tag{96b}$$

$$E^n_{k+1,2} = \alpha_m(n\Delta t)A_m \exp(\mathrm{i}m(k+1)\Delta x). \tag{96c}$$

We also define the growth rate between the steps as

$$g_m = \frac{\alpha_m((n+1)\Delta t)}{\alpha_m(n\Delta t)}. \tag{97}$$

Under the Fourier decomposition, the weighted average $\breve{E}_{k,2}$ becomes

$$\breve{E}^n_{k,2} = \alpha_m(n\Delta t)A_m \exp(\mathrm{i}mk\Delta x)\left(\frac{1}{6}\exp(\mathrm{i}m\Delta x) + \frac{2}{3} + \frac{1}{6}\exp(-\mathrm{i}m\Delta x)\right). \tag{98}$$

Now Eq. (95) is

$$\frac{g_m - 1}{c\Delta t}\left(\frac{1}{6}\exp(\mathrm{i}m\Delta x) + \frac{2}{3} + \frac{1}{6}\exp(-\mathrm{i}m\Delta x)\right) = \frac{1}{3\sigma\Delta x}(\exp(\mathrm{i}m\Delta x) - 2 + \exp(-\mathrm{i}m\Delta x)). \tag{99}$$

This equation can be simplified using the following definition:

$$2\cos(m\Delta x) = \exp(\mathrm{i}m\Delta x) + \exp(-\mathrm{i}m\Delta x). \tag{100}$$

Eq. (99) then reduces to

$$\frac{g_m - 1}{c\Delta t}\left(\frac{2}{3} + \frac{1}{3}\cos(m\Delta x)\right) = \frac{2}{3\sigma\Delta x}(\cos(m\Delta x) - 1). \tag{101}$$

The growth rate is then

$$g_m = 1 + \frac{2c\Delta t}{3\sigma\Delta x}\frac{\cos(m\Delta x) - 1}{\frac{2}{3} + \frac{1}{3}\cos(m\Delta x)}. \tag{102}$$

This equation is equivalent to

$$g_m = 1 + 2vC, \tag{103}$$

where we have defined

$$v = \frac{c\Delta t}{3\sigma\Delta x^2}, \tag{104}$$

$$C = \frac{\cos(m\Delta x) - 1}{\frac{2}{3} + \frac{1}{3}\cos(m\Delta x)}. \tag{105}$$

The magnitude of g_m is largest when $C = -6$, a situation that makes Eq. (103)

$$|g_m| \leqslant |1 - 12v|. \tag{106}$$

Setting $|g_m| = 1$ and solving for v yields $v = \{0, 1/6\}$. At $v = 1/6$ the slope of $|g_m|$ is positive. This fact means that if v is less than 1/6, the growth rate is stable. The stability condition is then

$$\frac{1}{3\sigma\Delta x}\frac{c\Delta t}{\Delta x} \leqslant \frac{1}{6}. \tag{107}$$

This expression is a CFL condition for an explicit diffusion equation, and it is less restrictive than the streaming-limit time-step limit of Eq. (62) for optically thick problems. This condition is less restrictive because in the diffusion limit we scale $\sigma\Delta x$ as $O(\epsilon^{-1})$. The time step allowed by Eq. (107) will be greater than the streaming limit as long as $\sigma\Delta x > 2/3$. Klar's method [16,17] has a CFL limit similar to the one above except with the right side being 1/2 rather than 1/6.

We note that in our implementation, to solve a problem that has optically thick and optically thin regions we are forced to use the more restrictive hyperbolic CFL limit of Eq. (62).

9. Numerical results

In our numerical results, unless otherwise stated we have chosen the time step based on the formula

$$\Delta t = (\mathrm{CFL})\frac{\Delta t}{c}$$

with the most common choice being CFL = 0.3.

9.1. Streaming in a vacuum

The first problem we test our method on has photons propagating through a vacuum. In this problem we use P_1, and on the left boundary we specify the incoming characteristics corresponding to $\psi_0 = \psi_1 = 1$; this boundary condition is a P_1 approximation to a right-going beam. On the right boundary we specify that the incoming characteristics are zero.

The exact P_1 solution to this problem is $\psi_0 = 0.5(1 + \sqrt{3})h(x - ct)$, where $h(z)$ is the Heaviside step function. Fig. 2 shows the effect of changing the slope limiter on the solution. Without a slope limiter, there are

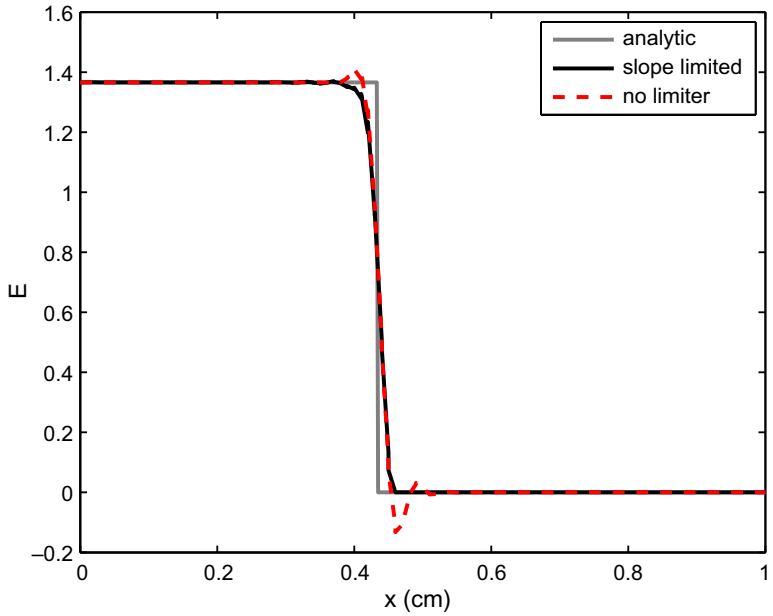

Fig. 2. Vacuum propagation problem solutions at $t = 2.5 \times 10^{-11}$ s for the double minmod limiter versus the unlimited solution. These are all P_1 solutions with $\Delta x = 0.01$ cm and $\Delta t = 1 \times 10^{-13}$ s (CFL = 0.3).

oscillations that allow the energy density to become less than zero. The limiter eliminates these oscillations. We note that if the energy density is negative in a problem with non-zero opacity, the material temperature could become negative and cause problems with the equation of state of the material.

9.2. Diffusive Marshak-wave problem

The next problem we examine is a Marshak-wave problem consisting of a semi-infinite medium of material with an opacity given by $\sigma = 300/T^3$, where the units of σ are cm^{-1} and T are keV. We specify an incoming isotropic distribution corresponding to a 1 keV temperature source on the boundary at $x = 0$; there is no incoming radiation on the right boundary. The heat capacity in this problem is constant with a value of 0.3×10^{16} erg/ cm^3/keV. There is a semi-analytic equilibrium–diffusion solution, and we compare this solution to the numerical results. In this problem, we expect the diffusion solution and the transport solution to be the same because the problem is so absorption dominated that the material energy and radiation energy should be in equilibrium. For our numerical solution we use an initial condition of $T(x,0) = 10^{-9}$ keV and $E(x,0) = ac(T(x,0))^4$.

Fig. 3 shows numerical results compared to the semi-analytic solution for the Marshak-wave problem. The numerical solution uses a optically thick spatial grid with each cell spanning at minimum 9 mean-free paths and as many as 4.8×10^{30} mean-free paths. In the 10.0×10^{-8} s solution the average cell thickness is 37 mean-free paths. We do not use larger cells because a coarser grid can not resolve the shape of the solution.

To get the numerical solutions in Fig. 3, we used a time step 10 times the CFL limit for the pure streaming problem (see Eq. (62)). We choose this time step based on the fact that our asymptotic analysis applies to this problem and in this limit, we have a larger time-step restriction given by Eq. (107).

9.3. Marshak wave in thin medium

Fig. 4 shows numerical results from an identical Marshak-wave problem except with an optically thinner background medium ($\sigma = 3/T^3$ cm^{-1}). This figure gives the radiation temperature as $\sqrt[4]{E/c}$. In this thin prob-

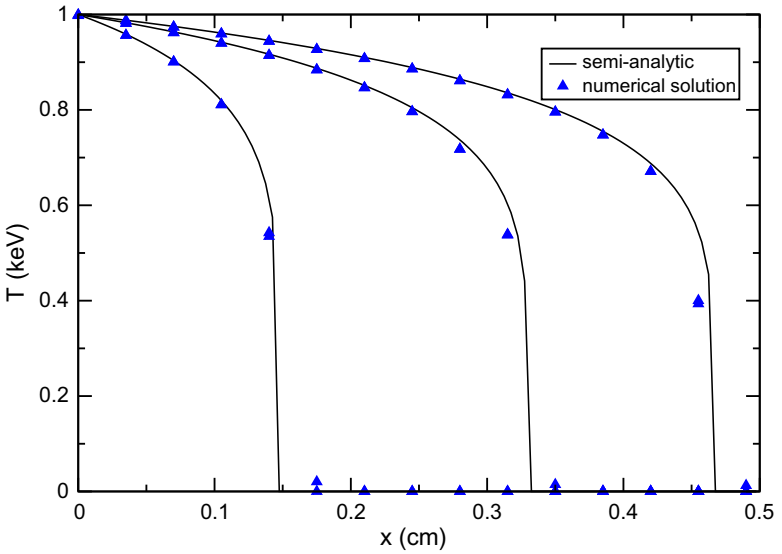

Fig. 3. Marshak-wave problem solutions for the material temperature at 1.0×10^{-8} s, 5.0×10^{-8} s, and 10.0×10^{-8} s respectively. The solid lines are the semi-analytic solutions, the triangles are the nodal values of a numerical solution. The numerical solutions were computed using P_5, $\Delta x = 0.035$ cm, $\Delta t = 4.0 \times 10^{-12}$ s (CFL ≈ 3.43). This time step is 10 times the largest possible time step in the streaming limit.

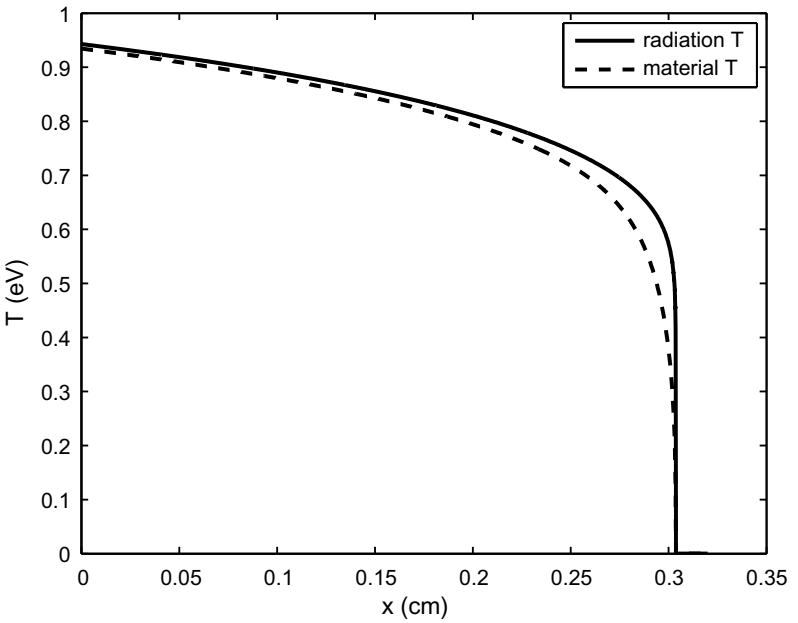

Fig. 4. Material and radiation temperature solutions to the thin Marshak-wave problem at $t = 1 \times 10^{-9}$ s. These results were obtained with P_1, $\Delta x = 1.5625 \times 10^{-4}$ cm, and CFL $= 0.3$.

lem there are transport effects, and the diffusion solution is not adequate. We compare different P_N approximations to a P_{99} solution in Fig. 5. Our error is quantified using the L_2 norm

$$L_2(T - T_{\text{ref}}) = \sqrt{\frac{1}{2N_x}\sum_{k=1}^{N_x}\sum_{i=1}^{2}(T_{k,i} - T_{\text{ref},k,i})^2}, \tag{108}$$

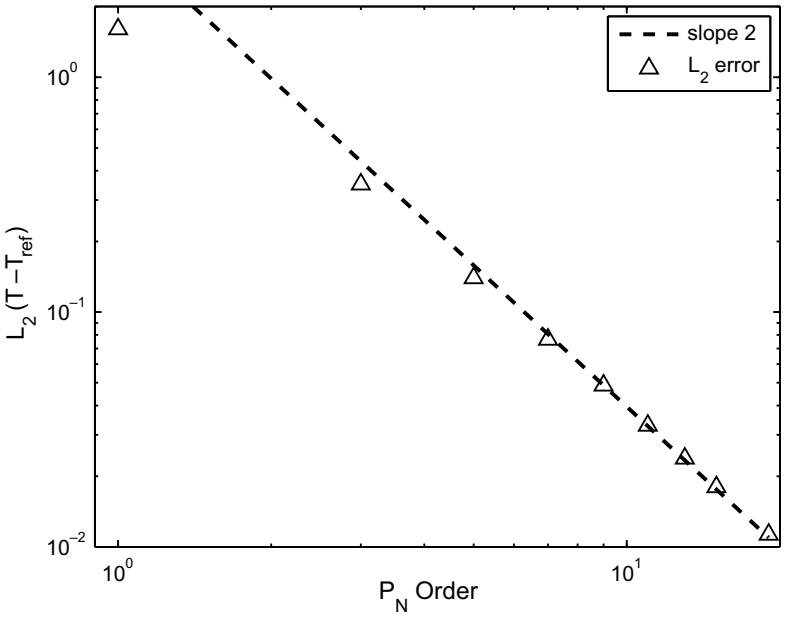

Fig. 5. Error in different P_N approximations as compared to the P_{99} solution. All numerical solutions used $\Delta x = 5 \times 10^{-3}$ cm and CFL = 0.3.

where N_x is the number of spatial cells and the sum over i represents the unknowns in a cell. In this problem the error in the P_N expansion decreases as $O(N^2)$ as N increases. For an infinitely smooth function, the convergence rate of the spherical harmonics expansion is exponential. The fact that in this problem the convergence rate is second order suggests that the radiation intensity is non-smooth in its third derivative with respect to the direction of flight, μ.

Using this thin problem also allows us to measure the error convergence for the spatial scheme. To measure the error we use an L_2 norm given by the following formula:

$$L_2(T - T_{\text{ref}}) = \sqrt{\frac{1}{N_x}\sum_{k=1}^{N_x}(T_k^{\text{avg}} - T_{\text{ref},k}^{\text{avg}})^2} \tag{109}$$

with

$$T_k^{\text{avg}} = \frac{1}{2}(T_{k,1} + T_{k,2}). \tag{110}$$

We use cell averages because we want to project the reference solution onto coarser grids. Each numerical solution has $N_x = 2^m$ for some positive integer m. Our reference solution has $N_x = 2048$ ($m = 11$). Fig. 6 shows that the method is first order on the thin Marshak-wave problem. This problem has a non-smooth solution that is causing the method to have first-order convergence in space.

9.4. "Smooth" Marshak wave

The standard Marshak wave is not a good problem to show the order of accuracy of a method because the solution is not smooth. A better problem to demonstrate the order of accuracy of our semi-implicit method has a smooth initial condition of

$$E(x,0) = ac + (ac - 0.04)\frac{1 + \tanh[50(x - 0.25)]}{2} \tag{111}$$

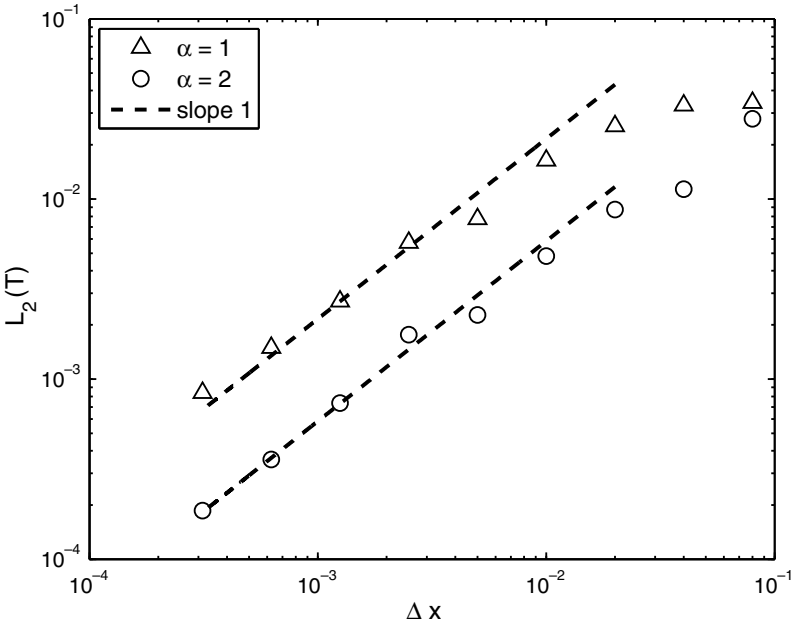

Fig. 6. Temperature–error convergence in Δx for the P_1 solution to the thin Marshak-wave problem with CFL = 0.3 with different slope limiters.

and

$$T(x,0) = \left(\frac{E(x,0)}{ac}\right)^{1/4}. \tag{112}$$

This initial condition was previously used by Lowrie to analyze time-discretization schemes for the diffusion equation [21]. The boundary conditions are the same as for the previous Marshak-wave problems and we have $\sigma = 3/T^3$ cm. Given this form of σ the problem has regions that are diffusive and optically thick (the cold

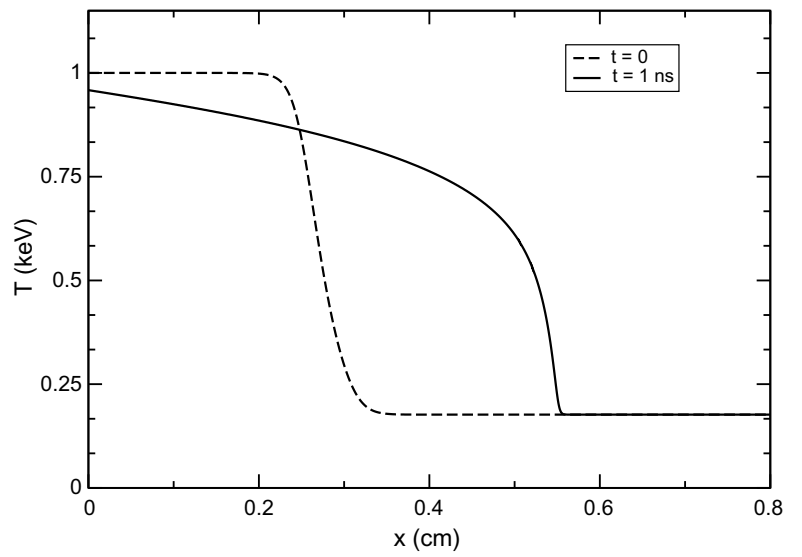

Fig. 7. Temperature initial condition and solution at 1×10^{-9} s for the smooth wave problem. The solution has $\Delta x = 4 \times 10^{-4}$ cm and CFL = 0.3.

regions of the problem) as well as optically thin regions where the material temperature is higher. The initial condition and solution to this problem at $t = 1 \times 10^{-9}$ s are shown in Fig. 7.

Solutions using different values of Δx are shown in Fig. 8. Upon inspecting these results, we see that the impact of refining the spatial grid is superior tracking of the wavefront. The slowly varying part of the solution is captured accurately for all cell sizes shown; it takes smaller mesh spacing to correctly place the wavefront. The detail of this wavefront is shown in Fig. 9.

The L_2 error convergence results are shown in Fig. 10. The error in this case is the difference between a solution and the reference solution with $N_x = 2048$. The procedure for calculating the error is the same as in the convergence study above. The results on this convergence plot shows that the error convergence approaches

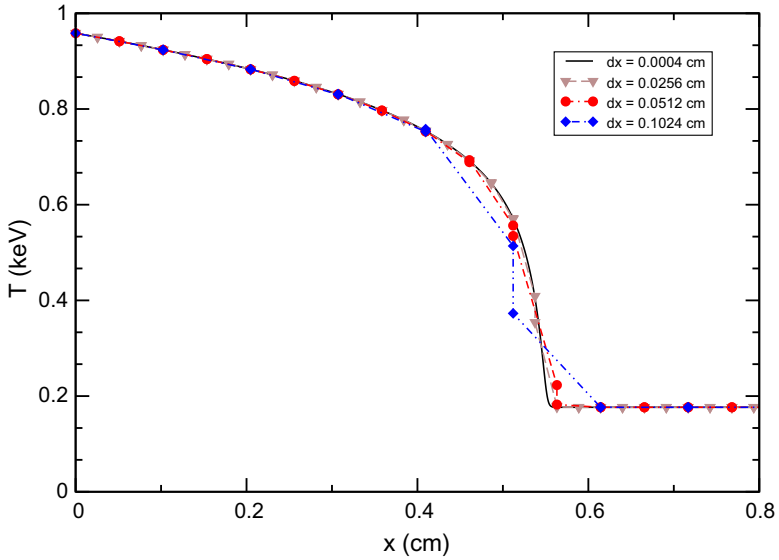

Fig. 8. Nodal values of the material temperature at 1×10^{-9} s for the smooth wave problem with CFL = 0.3 and different values of Δx.

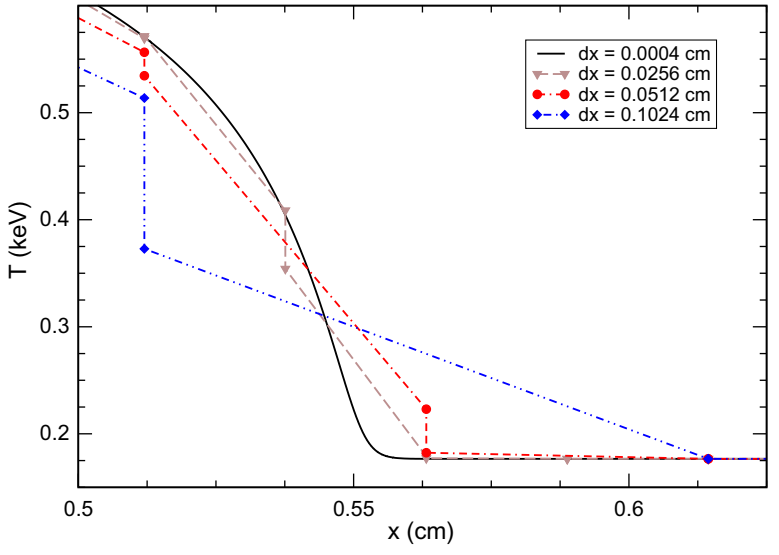

Fig. 9. Detail of the wavefront in the smooth wave problem at 1×10^{-9} s.

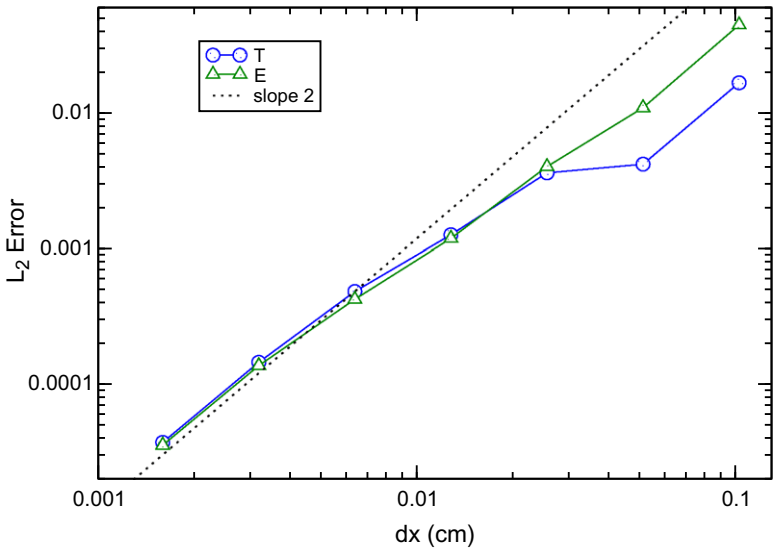

Fig. 10. L_2 error convergence for the smooth wave problem. All solutions had CFL = 0.3.

second order as the cell size and time step are decreased. In these results we had to obey the hyperbolic CFL condition because there are optically thin regions in the problem. Despite having to obey this more restrictive condition, we do observe second-order error convergence in time, whereas in diffusive problems our time integration error decays only at first order.

10. Conclusions

We have presented a linear discontinuous Galerkin method for the P_N equations. Our method uses a semi-implicit time-integration scheme that treats the streaming terms explicitly with second-order accurate Runge–Kutta and the material-coupling implicitly with backward Euler and a linearized emission source. The benefit of this approach is that each time step can be computed cheaply at the expense of having a CFL restriction for the time-step size.

Our method does preserve the asymptotic diffusion limit of the radiative transfer system: a fact that we demonstrated through analysis and numerical results. Previous upwind P_N methods that used a finite volume approach did not have this property [15]. Also, in this limit, the CFL limit is relaxed, and we produced accurate results for a diffusive Marshak-wave problem at 10 times the CFL limit for the unscaled equations. In the future we will examine the DG method in two and three dimensions to confirm that the method retains the asymptotic diffusion limit.

On an optically thin Marshak-wave problem, the method converged at a second-order rate in the order of the P_N expansion and is first-order accurate in space and time. Although we would expect our method to be second order as Δx and Δt are decreased, this convergence rate was not observed for this problem. This result was most likely due to the non-smooth wavefront of the solution in this problem. We were able to show second-order convergence for both the radiation energy density and the material temperature in an optically thin problem with a smooth initial condition. On these problems away from the diffusion limit we must obey a hyperbolic CFL restriction on the time step size.

We plan on extending this method to multiple dimensions to ferret out the possible efficiencies of the semi-implicit approach. We believe that some of the problems encountered by other transport methods in parallel, multi-dimensional simulations can be addressed using our scheme. For the above method, domain decomposition and complicated mesh structures (for example dendritic meshes or non-convex cells) do not appear to pose significant problems. If this postulate holds true in practice, our method will be a competitive means for solving large-scale radiative-transfer problems – despite the speed-of-light-based CFL restriction.

Appendix A. The P_3 and P_5 equations

A.1. P_3 equations

The P_3 equations have the following definitions for $\mathbf{u}$, $\mathbf{A}$, and $\mathbf{q}$:

$$\mathbf{u} = \begin{pmatrix} \psi_0 \\ \psi_1 \\ \psi_2 \\ \psi_3 \end{pmatrix}, \quad \mathbf{A} = \begin{pmatrix} 0 & 1 & 0 & 0 \\ \frac{1}{3} & 0 & \frac{2}{3} & 0 \\ 0 & \frac{2}{5} & 0 & \frac{3}{5} \\ 0 & 0 & \frac{3}{7} & 0 \end{pmatrix}, \quad \mathbf{q} = \begin{pmatrix} \sigma(acT^4 - \psi_0) \\ -\sigma\psi_1 \\ -\sigma\psi_2 \\ -\sigma\psi_3 \end{pmatrix}. \tag{A.1}$$

The eigenvalue/eigenvector matrices of $\mathbf{A}$ for this system are

$$\mathbf{\Lambda} = \begin{pmatrix} -0.861136 & 0 & 0 & 0 \\ 0 & 0.861136 & 0 & 0 \\ 0 & 0 & -0.339981 & 0 \\ 0 & 0 & 0 & 0.339981 \end{pmatrix}, \tag{A.2}$$

$$\mathbf{R} = \begin{pmatrix} -3.28141 & 3.28141 & 2.42879 & -2.42879 \\ 2.82574 & 2.82574 & -0.825742 & -0.825742 \\ -2.00932 & 2.00932 & -0.793289 & 0.793289 \\ 1 & 1 & 1 & 1 \end{pmatrix}, \tag{A.3}$$

$$\mathbf{R}^{-1} = \begin{pmatrix} -0.0530038 & 0.136931 & -0.16228 & 0.113069 \\ 0.0530038 & 0.136931 & 0.16228 & 0.113069 \\ 0.134253 & -0.136931 & -0.219248 & 0.386931 \\ -0.134253 & -0.136931 & 0.219248 & 0.386931 \end{pmatrix}. \tag{A.4}$$

For P_3, it is useful to have the following matrix:

$$\frac{1}{2}|\mathbf{A}| = \begin{pmatrix} 0.260634 & 0 & 0.277519 & 0 \\ 0 & 0.371641 & 0 & 0.166512 \\ 0.0555039 & 0 & 0.339925 & 0 \\ 0 & 0.0713621 & 0 & 0.228917 \end{pmatrix}. \tag{A.5}$$

A.2. P_5 equations

The P_5 equations have the following definitions for $\mathbf{u}$, $\mathbf{A}$, and $\mathbf{q}$:

$$\mathbf{u} = \begin{pmatrix} \psi_0 \\ \psi_1 \\ \psi_2 \\ \psi_3 \\ \psi_4 \\ \psi_5 \end{pmatrix}, \quad \mathbf{A} = \begin{pmatrix} 0 & 1 & 0 & 0 & 0 & 0 \\ \frac{1}{3} & 0 & \frac{2}{3} & 0 & 0 & 0 \\ 0 & \frac{2}{5} & 0 & \frac{3}{5} & 0 & 0 \\ 0 & 0 & \frac{3}{7} & 0 & \frac{4}{7} & 0 \\ 0 & 0 & 0 & \frac{4}{9} & 0 & \frac{5}{9} \\ 0 & 0 & 0 & 0 & \frac{5}{11} & 0 \end{pmatrix}, \quad \mathbf{q} = \begin{pmatrix} \sigma(acT^4 - \psi_0) \\ -\sigma\psi_1 \\ -\sigma\psi_2 \\ -\sigma\psi_3 \\ -\sigma\psi_4 \\ -\sigma\psi_5 \end{pmatrix}. \tag{A.6}$$

The eigenvalue/eigenvector matrices of $\mathbf{A}$ for this system are

$$\mathbf{\Lambda} = \begin{pmatrix} -0.93247 & 0 & 0 & 0 & 0 & 0 \\ 0 & 0.93247 & 0 & 0 & 0 & 0 \\ 0 & 0 & -0.661209 & 0 & 0 & 0 \\ 0 & 0 & 0 & 0.661209 & 0 & 0 \\ 0 & 0 & 0 & 0 & -0.238619 & 0 \\ 0 & 0 & 0 & 0 & 0 & 0.238619 \end{pmatrix}, \tag{A.7}$$

$$\mathbf{R} = \begin{pmatrix} -4.86116 & 4.86116 & 3.39679 & -3.39679 & -2.98847 & 2.98847 \\ 4.53288 & 4.53288 & -2.24599 & -2.24599 & 0.713107 & 0.713107 \\ -3.90958 & 3.90958 & 0.529209 & -0.529209 & 1.239 & -1.239 \\ 3.05402 & 3.05402 & 0.914129 & 0.914129 & -0.968151 & -0.968151 \\ -2.05143 & 2.05143 & -1.45466 & 1.45466 & -0.524962 & 0.524962 \\ 1 & 1 & 1 & 1 & 1 & 1 \end{pmatrix}, \tag{A.8}$$

$$\mathbf{R}^{-1} = \begin{pmatrix} -0.0176218 & 0.0492953 & -0.0708614 & 0.0774962 & -0.0669285 & 0.0398752 \\ 0.0176218 & 0.0492953 & 0.0708614 & 0.0774962 & 0.0669285 & 0.0398752 \\ 0.0531034 & -0.105337 & 0.0413664 & 0.100037 & -0.204672 & 0.171967 \\ -0.0531034 & -0.105337 & -0.0413664 & 0.100037 & 0.204672 & 0.171967 \\ -0.0782864 & 0.0560419 & 0.162284 & -0.177533 & -0.123768 & 0.288158 \\ 0.0782864 & 0.0560419 & -0.162284 & -0.177533 & 0.123768 & 0.288158 \end{pmatrix}. \tag{A.9}$$

In addition we have

$$\frac{1}{2}|\mathbf{A}| = \begin{pmatrix} 0.254974 & 0 & 0.298390 & 0 & -0.0680521 & 0 \\ 0 & 0.374329 & 0 & 0.148788 & 0 & -0.0378067 \\ 0.0596779 & 0 & 0.320784 & 0 & 0.135782 & 0 \\ 0 & 0.0637664 & 0 & 0.322171 & 0 & 0.150928 \\ -0.00756134 & 0 & 0.0754342 & 0 & 0.340391 & 0 \\ 0 & -0.0103109 & 0 & 0.0960452 & 0 & 0.219649 \end{pmatrix} \tag{A.10}$$

References

[1] J.S. Warsa, T.A. Wareing, J.E. Morel, Krylov iterative methods and the degraded effectiveness of Diffusion Synthetic Acceleration for multidimensional S_N calculations in problems with material discontinuities, Nucl. Sci. Eng. 147 (2004) 218–248.

[2] J.A. Fleck Jr., J.D. Cummings, An implicit Monte Carlo scheme for calculating time and frequency dependent nonlinear radiation transport, J. Comput. Phys. 8 (1971) 313–342.

[3] J.E. Morel, B.T. Adams, T. Noh, J.M. McGhee, T.M. Evans, T.J. Urbatsch, Spatial discretizations for self-adjoint forms of the radiative transfer equations, J. Comput. Phys. 214 (2006) 12–40.

[4] J.E. Morel, T.A. Wareing, R.B. Lowrie, D.K. Parsons, Analysis of ray-effect mitigation techniques, Nucl. Sci. Eng. 144 (1) (2003) 1–22.

[5] I. Perugia, D. Schoetzau, J. Warsa, On a discontinuous Galerkin method for radiation–diffusion problems, in: M. Feistauer (Ed.), Numerical Mathematics and Advanced Applications: ENUMATH 2003, Springer, 2004, pp. 687–697.

[6] R.G. McClarren, J.P. Holloway, T.A. Brunner, On solutions to the P_n equations for thermal radiative transfer, J. Comput. Phys. 227 (2008) 2864–2885.

[7] R.G. McClarren, J.P. Holloway, T.A. Brunner, T.A. Mehlhorn, A quasi-linear implicit Riemann solver for the time-dependent P_n equations, Nucl. Sci. Eng. 155 (2007) 290–299.

[8] R.G. McClarren, Spherical harmonics methods for thermal radiation transport, Ph.D. Thesis, University of Michigan, Ann Arbor, MI, 2007.

[9] R. McClarren, J.P. Holloway, T. Brunner, T. Mehlhorn, Implicit Riemann solvers for the P_n equations, in: F. Graziani (Ed.), Computational Methods in Transport, Lecture Notes in Computational Science and Engineering, vol. 48, Springer, 2006.

[10] R.G. McClarren, J.P. Holloway, A quasi-linear implementation of high resolution time integration for the P_n equations, Nucl. Sci. Eng. 159 (2008) 330–337.
[11] T.A. Brunner, J.P. Holloway, Two dimensional time dependent Riemann solvers for neutron transport, J. Comput. Phys. 210 (1) (2005) 386–399.
[12] W. Reed, T. Hill, Triangular mesh methods for the neutron transport equation, Tech. Rep. LA-UR-73-479, Los Alamos Scientific Laboratory, 1973.
[13] B. Cockburn, C. Shu, TVB Runge–Kutta projection discontinuous Galerkin finite element method for conservation laws II: General framework, Math. Comput. 52 (186) (1989) 411–435.
[14] R.B. Lowrie, J.E. Morel, Discontinuous Galerkin for hyperbolic systems with stiff relaxation, in: B. Cockburn, G.E. Karniadakis (Eds.), Discontinuous Galerkin Methods: Theory, Computation and Applications, Springer, 2000, pp. 385–390.
[15] R. McClarren, J.P. Holloway, T.A. Brunner, Establishing an asymptotic diffusion limit for Riemann solvers on the time-dependent P_N equations, in: International Topical Meeting on Mathematics and Computation, Supercomputing, Reactor Physics and Nuclear and Biological Applications, American Nuclear Society, Avignon, France, 2005.
[16] A. Klar, An asymptotic-induced scheme for nonstationary transport equations in the diffusive limit, SIAM J. Numer. Anal. 35 (3) (1998) 1073.
[17] A. Klar, A. Unterreiter, Uniform stability of a finite difference scheme for transport equations in diffusive regimes, SIAM J. Numer. Anal. 40 (3) (2002) 891–913.
[18] G.C. Pomraning, The Equations of Radiation Hydrodynamics, Pergamon Press, Oxford, 1973.
[19] G.I. Bell, S. Glasstone, Nuclear Reactor Theory, Robert E. Kreiger Publishing, Malabar, FL, 1970.
[20] R.J. LeVeque, Numerical Methods for Conservation Laws, second ed., Birkhäuser Verlag, Basel, 1992.
[21] R.B. Lowrie, A comparison of implicit time integration methods for nonlinear relaxation and diffusion, J. Comput. Phys. 196 (2004) 566–590.
[22] M.L. Adams, Discontinuous finite element transport solutions in thick diffusive problems, Nucl. Sci. Eng. 137 (2001) 298–333.
[23] E.W. Larsen, J.E. Morel, W.F. Miller, Asymptotic solutions of numerical transport problems in optically thick, diffusive regimes, J. Comput. Phys. 69 (1987) 283–324.
[24] B. van Leer, Towards the ultimate conservative difference scheme IV. A new approach to numerical convection, J. Comput. Phys. 23 (3) (1977) 276–299.
[25] T.A. Brunner, J.P. Holloway, One-dimensional Riemann solvers and the maximum entropy closure, J. Quant. Spectros. Radiat. Transf. 69 (2001) 543–566.
[26] E. Larsen, G. Pomraning, V. Badham, Asymptotic analysis of radiative transfer problems, J. Quant. Spectros. Radiat. Transf. 29 (4) (1983) 285–310.
[27] J.D. Densmore, E.W. Larsen, Asymptotic equilibrium diffusion analysis of time-dependent Monte Carlo methods for gray radiative transfer, J. Comput. Phys. 199 (2004) 175–204.
[28] J.E. Morel, T.A. Wareing, K. Smith, A linear-discontinuous spatial differencing scheme for S_N radiative transfer calculations, J. Comput. Phys. 128 (1996) 445–462.
[29] M.L. Adams, P.F. Nowak, Asymptotic analysis of a computational method for time- and frequency-dependent radiative transfer, J. Comput. Phys. 146 (1998) 366–403.
[30] E.W. Larsen, J.E. Morel, Asymptotic solutions of numerical transport problems in optically thick, diffusive regimes II, J. Comput. Phys. 83 (1989) 212–236.
[31] C.W. Curtis, Linear Algebra, Springer-Verlag, New York, 1984.
[32] J.C. Strikwerda, Finite Difference Schemes and Partial Differential Equations, second ed., Society for Industrial and Applied Mathematics (SIAM), 2004.